

Midline radial glia translocation and corpus callosum formation require FGF signaling

Karen Müller Smith^{1,4}, Yasushi Ohkubo^{1,4}, Maria Elisabetta Maragnoli¹, Mladen-Roko Rašin^{2,3}, Michael L Schwartz², Nenad Šestan^{2,3} & Flora M Vaccarino^{1,2}

Midline astroglia in the cerebral cortex develop earlier than other astrocytes through mechanisms that are still unknown. We show that radial glia in dorsomedial cortex retract their apical endfeet at midneurogenesis and translocate to the overlying pia, forming the indusium griseum. These cells require the fibroblast growth factor receptor 1 (*Fgfr1*) gene for their precocious somal translocation to the dorsal midline, as demonstrated by inactivating the *Fgfr1* gene in radial glial cells and by RNAi knockdown of *Fgfr1* *in vivo*. Dysfunctional astroglial migration underlies the callosal dysgenesis in conditional *Fgfr1* knockout mice, suggesting that precise targeting of astroglia to the cortex has unexpected roles in axon guidance. FGF signaling is sufficient to induce somal translocation of radial glial cells throughout the cortex; furthermore, the targeting of astroglia to dorsolateral cortex requires FGFR2 signaling after neurogenesis. Hence, FGFs have an important role in the transition from radial glia to astrocytes by stimulating somal translocation of radial glial cells.

Radial glial progenitor cells of the cortical ventricular zone extend an apical foot to the ventricular surface and a basal process to the pial membrane. After their neurogenic phase (around embryonic day (E) 18.5 in mice), these cells begin translocating their cell bodies toward the pia and differentiate into astrocytes^{1–3}. Cortical astrocytes upregulate the intermediate filament glial fibrillary acidic protein (GFAP) several days after birth. However, astroglial cells at the telencephalic midline have been observed to develop GFAP immunostaining by E17.5, much earlier than other astrocytes^{4,5}. These cells populate the indusium griseum, the glial wedge and the midline zipper. The indusium griseum is composed of neurons and astrocytes located underneath the pial membrane of the dorsomedial pallium, above the path of the corpus callosum. The glial wedge is formed by radial glial cell bodies arranged in the medial pallial ventricular zone, underneath the indusium griseum⁶. The correct morphogenesis of these pioneer glial populations along the midline is thought to be crucial for guiding the axons of the developing corpus callosum^{6–8}.

The factors that drive the transformation of radial glia into astrocytes at the appropriate stage in development have not been elucidated. Cells of the glial wedge and indusium griseum are born as early as E13.5 and E14.5, respectively⁴. Before expressing GFAP, cells of the glial wedge express glutamate astrocyte transporter (*Glast/Slc1a3*), brain lipid binding protein (*Blbp/Fabp7*) and nestin (*Nes*) gene products typical of radial glial cells⁹, in keeping with their radial glial identity⁴. Hence, it is possible that cells of the indusium griseum derive from these radial glial progenitors that migrate to the cortical midline. If that were true, indusium griseum astroglia, unlike other cortical astrocytes, must be generated synchronously with upper layer cortical plate neurons and

must start their migratory process concurrently with neurons and much earlier than the astrocytes that populate other regions of the telencephalon. How the precise timing of migration and cortical targeting of these different populations of astroglial cells is regulated is unknown.

Previous *in vitro* studies have implicated the neuropeptide FGF2, a member of the fibroblast growth factor (FGF) family, in rendering progenitor cells competent to switch from neuronal to glial cell fates^{10–12}. Here, we show that the FGF receptor 1 gene (*Fgfr1*) is required for the early translocation of radial glial cells to the medial pallium, the prospective indusium griseum region, and that *Fgfr2* is required for the targeting of astroglia to the cerebral cortex at the end of gestation. In vertebrates, FGFs encompass 22 ligands¹³ that bind to 4 tyrosine kinase FGF receptors (FGFR1–4)¹⁴. FGFs are required for progenitor proliferation, specification and survival at early stages of CNS development^{12,15–20}. FGF receptors are widely expressed by telencephalic progenitors at these early stages^{16,21}. We and others found that at later stages of development, *Fgfr1* continues to be expressed in radial glial cells of the dorsomedial ventricular zone, in the hippocampal primordium and, as shown here, in its anterior rudiment, the indusium griseum. On the other hand, *Fgfr2* is expressed by radial glial cells of the dorsolateral ventricular zone and ganglionic eminences^{21,22}. The targeted inactivation of the *Fgfr1* gene within radial glial cells produces alterations in hippocampal development²³. We report here that these mice also show a prominent dysgenesis of the dorsal telencephalic commissures, including the corpus callosum and hippocampal commissure, without other obvious connectivity defects. In humans, homozygous inactivating mutations in the *FGFR1* gene

¹Child Study Center, ²Department of Neurobiology and ³Kavli Institute for Neuroscience, Yale University School of Medicine, New Haven, Connecticut 06520, USA. ⁴These authors contributed equally to this work. Correspondence should be addressed to F.M.V. (flora.vaccarino@yale.edu).

Received 3 April; accepted 24 April; published online 21 May 2006; doi:10.1038/nn1705

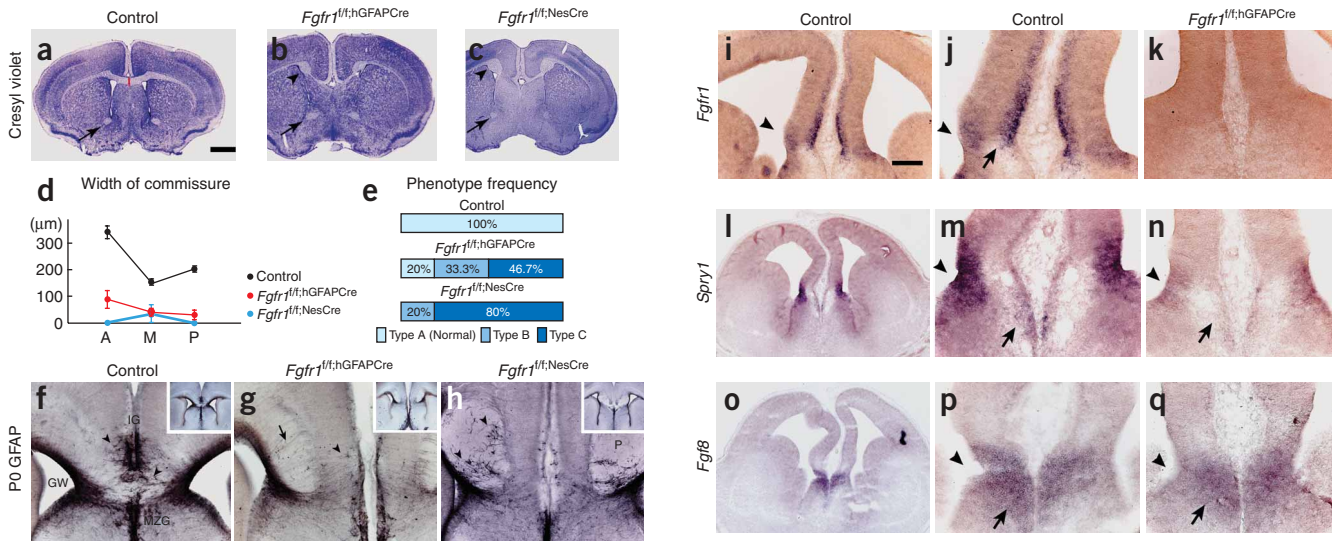


Figure 1 Disruption of dorsal telencephalic commissures in glial-specific *Fgfr1* mutant mice and enriched expression of FGF-related genes in anterior midline. (a–c) Cresyl violet–stained sections illustrating the most severe and common phenotype of *Fgfr1^{fl/f;hGFAPCre}* (b) and *Fgfr1^{fl/f;NesCre}* (c) mice as compared to Cre⁻ controls harboring *Fgfr1^{fl/f}* alleles (a). Arrowheads, Probst bundles; red line, corpus callosum; arrows, anterior commissure. Scale bar, 1 mm. (d) Commissure widths for anterior (A), medial (M) and posterior (P) cortical areas in control ($n = 17$), *Fgfr1^{fl/f;hGFAPCre}* ($n = 15$) and *Fgfr1^{fl/f;NesCre}* ($n = 5$) mice. (e) Frequency histogram categorizing mice into type A (normal), type B (commissures measuring <50% of normal in one or more area) or type C (commissures completely absent). (f–h) GFAP immunostaining in coronal sections of control (f), *Fgfr1^{fl/f;hGFAPCre}* (g) and *Fgfr1^{fl/f;NesCre}* (h) mice at P0 to visualize the glial wedge (GW), indusium griseum (IG) and midline zipper glia (MZG). Arrowheads, GFAP⁺ cells; P, Probst bundles; black arrow, radial glial fibers. (i–q) Expression of FGF-related genes in the anterior telencephalic midline at E14.5. *In situ* hybridization for *Fgfr1* in control (i,j) and *Fgfr1^{fl/f;hGFAPCre}* mice (k). Arrow, indusium griseum; arrowhead, glial wedge. *In situ* hybridization for *Spry1* in control mice (l,m) and *Fgfr1^{fl/f;hGFAPCre}* mice (n). *In situ* hybridization for *Fgf8* in control mice (o,p) and *Fgfr1^{fl/f;hGFAPCre}* mice (q). *Fgf8* expression was maintained in *Fgfr1^{fl/f;hGFAPCre}* mice (q). Scale bars: 200 μm in f–h, 200 μm in i, 400 μm in l and o, 100 μm in j,k,m,n,p and q.

result in Kallman syndrome with agenesis of the corpus callosum²⁴. Hence, the role for *Fgfr1* in midline commissure development is evolutionarily conserved. Using mouse mutants that lack *Fgfr1* and/or *Fgfr2* in radial glia along with shRNA-mediated knockdown of *Fgfr1* and overexpression of FGF2 and FGF8 proteins in cortical explants, we demonstrate that commissural dysgenesis is secondary to a defective translocation of radial glial cells from the ventricular zone to the anterior pallial midline, an area that is normally enriched in FGF1 signaling. Misexpression of FGF proteins in other areas of the cortical plate was sufficient to prematurely induce the upward translocation of radial glial cell bodies, underscoring a wider requirement for FGF2 signaling in somal translocation throughout the cerebral cortex.

RESULTS

Loss of *Fgfr1* in radial glia causes callosal dysgenesis

Targeted inactivation of the *Fgfr1* gene in radial glia was accomplished via Cre-dependent recombination of the loxP-flanked *Fgfr1^f* allele²⁵. Cre was driven by a human *GFAP-Cre* transgene (*hGFAP-Cre*) active in telencephalic radial glial cells beginning at E13.5–E14.5 (refs. 23,26). Mice homozygous for the recombined *Fgfr1* null allele (referred to as *Fgfr1^{fl/f;hGFAPCre}*) lacked the corpus callosum and hippocampal commissure (Fig. 1 and Supplementary Fig. 1 online). These mice had Probst bundles, collections of tangled axons adjacent to the cortical midline (Fig. 1b, arrowheads). Whereas the defects in the corpus callosum and hippocampal commissure were quite severe in most of the Cre transgene-bearing mice, they did not lead to a complete agenesis of these structures in all the *Fgfr1^{fl/f;hGFAPCre}* mice examined. We therefore assessed a series of control and mutant littermate mice in order to examine both the penetrance and expressivity of this pheno-

type. The average midline width of commissures was markedly smaller in the *Fgfr1^{fl/f;hGFAPCre}* mice compared to controls (Fig. 1d). An analysis of variance (ANOVA) showed a significant effect of genotype on commissure width ($F_{1,90} = 123$; $P < 0.0001$), and a significant interaction between genotype and region ($P < 0.01$), in that anterior and posterior regions were significantly worse than the middle. Categorically, we found that 47% of the *Fgfr1^{fl/f;hGFAPCre}* mice ($n = 15$) had complete agenesis of the corpus callosum, and an additional 33% percent of these mutants had a severely dysgenic corpus callosum in the middle section, adjacent to the fimbria, that was less than 50% of the average width in the control mice ($n = 17$). Another 20% of the *Fgfr1^{fl/f;hGFAPCre}* mice were similar to control mice (Fig. 1e). In marked contrast to the dorsal commissures, the ventral commissures, such as the anterior and the habenular commissures, were not affected in *Fgfr1* mutant mice (arrows in Fig. 1a,b; Supplementary Fig. 1).

This partial phenotype could potentially be attributed to a late or incomplete recombination of the *Fgfr1* allele. To inactivate the *Fgfr1* gene at an earlier time point and in a broader distribution, we mated mice bearing the *Fgfr1^{fl/f}* alleles with a Cre strain driven by the CNS-specific nestin enhancer, which drives Cre recombination in all telencephalic neural precursors by E11.5 (ref. 27). The *Fgfr1^{fl/f;NesCre}* mice also showed defects in the dorsal telencephalic commissures but not in the ventral commissures (Fig. 1a,c and Supplementary Fig. 1). Scoring adult *Fgfr1^{fl/f;NesCre}* mice ($n = 5$) for midline defects demonstrated that 100% of the mutant mice had a complete absence of midline crossing at the most anterior and posterior regions examined; however, 20% of the *Fgfr1^{fl/f;NesCre}* mice had a small number of callosal fibers in the region above the hippocampal commissure (level 'M' in Fig. 1d). Hence, the defects were more penetrant in the

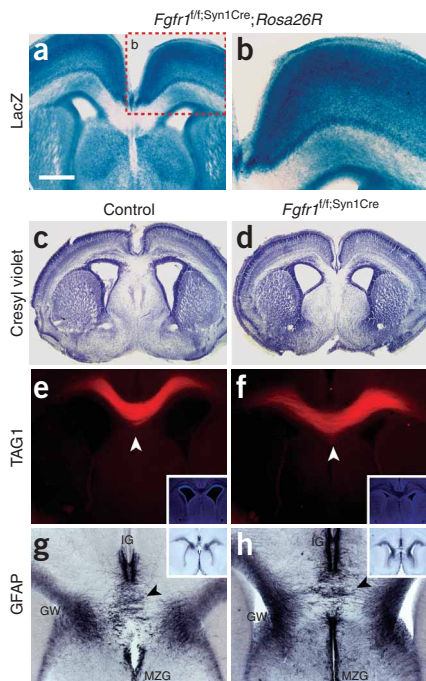


Figure 2 Normal corpus callosum and midline glia in mice lacking *Fgfr1* in neurons. (a) LacZ histochemistry in *Fgfr1^{fl/f};Syn1Cre;Rosa26R* mice showing the distribution of Cre recombinase activity at P0. (b) Magnification (2×) of the area framed in a. (c–h) Coronal 100-μm sections from control mouse brains (c,e,g) or from *Fgfr1^{fl/f};Syn1Cre* mice (d,f,h) stained with cresyl violet (c,d), TAG-1 (e,f) or GFAP (g,h). No abnormalities in commissure formation were detected in *Fgfr1^{fl/f};Syn1Cre* mutants (in e,f, white arrowheads point to crossing callosal fibers). Insets, low magnification 4,6-diamidino-2-phenylindole (DAPI) stain. Midline glial structures including the indusium griseum (IG), glial wedge (GW) and midline zipper glia (MZG) were indistinguishable in control (g) and *Fgfr1^{fl/f};Syn1Cre* mice (h). Insets, low magnification images. Scale bars: 400 μm in a,e and f, 800 μm in c and d, 200 μm in b, g and h.

Fgfr1^{fl/f};NesCre mice, although fewer mice with this mutation were examined (Fig. 1d,e).

Anterograde axonal tracing studies in adult mice using biotinylated dextran amines (BDA) stereotaxically injected into the frontal cortex demonstrated that both *Fgfr1^{fl/f};hGFAPCre* and *Fgfr1^{fl/f};NesCre* mice did not have any detectable labeling of axons within the contralateral cortex or white matter; instead, labeled cortical fibers were trapped within Probst bundles (Supplementary Fig. 2 online). However, corticostriatal and corticothalamic axon tracts in *Fgfr1^{fl/f};hGFAPCre* and *Fgfr1^{fl/f};NesCre* mice were similar to those in controls (Supplementary Fig. 2).

We next examined commissure development using lipophilic dye tracers. In 83% of *Fgfr1^{fl/f};hGFAPCre* mice, a complete loss of callosal axons from the motor and somatosensory cortex was already present at birth (controls, $n = 12$; *Fgfr1^{fl/f};hGFAPCre*, $n = 12$; Supplementary Fig. 2). There was also a loss of hippocampal commissural axons in neonatal *Fgfr1^{fl/f};hGFAPCre* mice (controls, $n = 6$; *Fgfr1^{fl/f};hGFAPCre*, $n = 3$; Supplementary Fig. 2). Furthermore, corticothalamic and corticostriatal projections were preserved in these mutant and control neonates (Supplementary Fig. 2). Together, these findings underscored a requirement for *Fgfr1* in the development of dorsal telencephalic commissures. Also, the presence of Probst bundles and the preserved corticostriatal and corticothalamic projections indicated that the defects were not due to a problem with axon extension or a general lack of neurite outgrowth.

Absent indusium griseum in glial-specific *Fgfr1* mutants

Commissural axon guidance is thought to depend upon the integrity of midline cells in the glial wedge, indusium griseum, midline zipper and glial sling. To examine the formation of these glial structures in *Fgfr1* mutant neonates, we performed immunohistochemistry for GFAP in knockout ($n = 6$) and control ($n = 6$) littermates at postnatal day (P) 0. The glial wedge, indusium griseum and midline zipper astroglia were clearly visible at this age in control mice throughout the anteroposterior extent of the telencephalon (Fig. 1f and Supplementary Fig. 1), as previously described⁴. In contrast, indusium griseum astroglia were absent in the anterior regions of the *Fgfr1^{fl/f};hGFAPCre* mice (Fig. 1g and

Supplementary Fig. 1). Furthermore, in mutants, the GFAP-positive (GFAP⁺) processes emerging from the glial wedge and adjacent ventricular zone remained attached at both the ventricular zone and the pia, and very few astrocytes were observed in between the glial wedge and the indusium griseum (Fig. 1g and Supplementary Fig. 1, black arrows). In comparison, in control littermates, GFAP⁺ astrocytes had already reached the indusium griseum or were noticeable in the region between the glial wedge and indusium griseum (Fig. 1f and Supplementary Fig. 1, arrowheads). The *Fgfr1^{fl/f};NesCre* mice had a more extensive defect in the morphogenesis of the indusium griseum, with posterior regions also lacking glial cells within this structure. There were no GFAP⁺ cell bodies migrating toward the indusium griseum; however, GFAP⁺ cells were seen in the glial wedge or appeared to be trapped within the Probst bundles (Fig. 1h and Supplementary Fig. 1, arrowheads). The uniform lack in accumulation of astroglial cells at the midline correlates with the more severe defect in callosal morphogenesis and may be a reflection of the more widespread *Fgfr1* recombination in radial glial cells driven by the nestin promoter.

FGF signaling is enriched at the anterior cortical midline

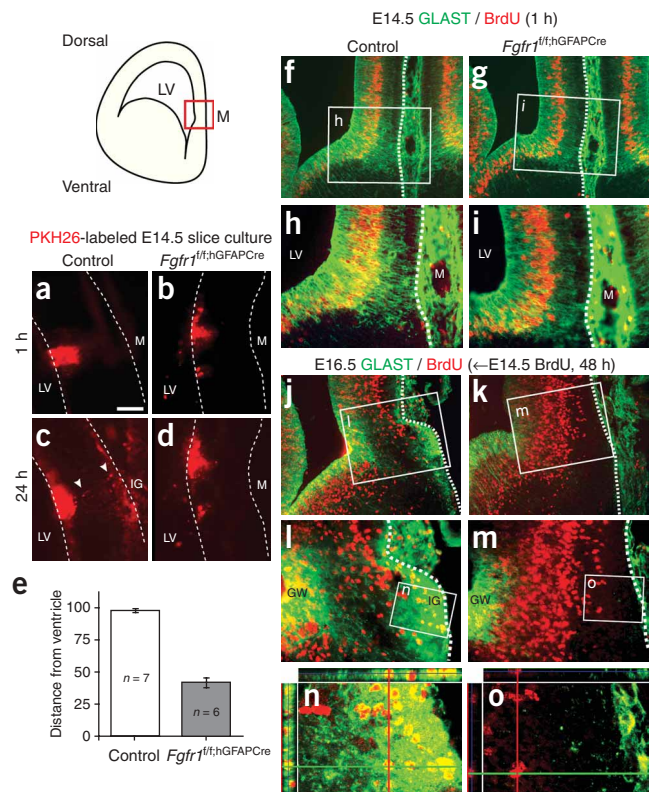
At E14.5, when a majority of indusium griseum cells undergo their last mitosis⁸, the highest expression of *Fgfr1* was in the dorsomedial portion of the ventricular zone (arrowhead in Fig. 1i), corresponding to the glial wedge, and in the primordium of the indusium griseum (arrow in Fig. 1j). *Fgfr1* was also expressed at lower levels in the cortical plate. This expression pattern remained essentially unchanged at E16.5, when a large proportion of pioneer neocortical axons project across the anterior midline (ref. 28 and data not shown). The expression of *Fgfr1* was undetectable in corresponding areas of *FGFR1^{fl/f};hGFAPCre* mice (Fig. 1k).

The restricted expression of *Fgfr1* may be attributable to the positive autoregulation of *Fgfr1* transcription via ligand-induced activation of FGFR1 signaling²³. Indeed, in control mice, the expression of *Spry1*, a gene product that is immediately downstream to the activation of FGF receptors^{15,29}, partially overlaps that of *Fgfr1* (Fig. 1l,m). The *Spry1* signal was highest in the glial wedge (Fig. 1m, arrowhead) with some expression in the indusium griseum (Fig. 1m, arrow). In both areas, the signal for *Spry1* was greatly reduced in *Fgfr1^{fl/f};hGFAPCre* mice (compare Fig. 1m with Fig. 1n).

FGF8, together with other FGF ligands, is enriched at the dorso-anterior midline at early stages of development^{20,30,31}. At E14.5 (Fig. 1o–q), *Fgfr8* mRNA was expressed within the presumptive glial wedge (arrowheads) and indusium griseum (arrows). Therefore, this secreted ligand is likely to form a concentration gradient emerging from this region. Notably, the expression pattern of *Fgfr8* was unchanged in the *Fgfr1^{fl/f};hGFAPCre* mice (Fig. 1q).

The presence of FGFR signaling molecules within the glial wedge, as well as in the presumptive indusium griseum, is consistent with the

Figure 3 Migration of astroglial cells to the indusium griseum is disrupted in glial-specific *Fgfr1* mutant. (a–e) Movement of PKH26-labeled cells from ventricular zone to midline pia in coronal slices of E14.5 mouse telencephalon. Labeled cells in the ventricular zone 1 h after labeling (a,b). White dashed lines, slice shape as determined by bright-field images. (c) Control slices at 24 h showing labeled cells (arrowheads) translocated toward the indusium griseum while little translocation occurred in *Fgfr1^{fl/f};hGFAP^{Cre}* slices (d). (e) Average distance from the ventricular wall to the leading edge of PKH-labeled cells after 24 h in culture, normalized by the cortical thickness (cells close to the pia would have a value of 100). Mean values are 97.8 in control ($n = 7$) and 41.2 in *Fgfr1^{fl/f};hGFAP^{Cre}* embryos ($n = 6$). $P < 10^{-5}$, one-tailed Student's *t*-test. (f–o) Coronal sections from control (f,h,j,l,n) and *Fgfr1^{fl/f};hGFAP^{Cre}* embryos (g,i,k,m,o) harvested 1 h (f–i) or 48 h (j–o) after a single BrdU administration at E14.5 and immunostained for GLAST (green) and BrdU (red). Dashed white lines, midline pia. Accumulation of GLAST⁺ and BrdU⁺ cells in the indusium griseum of control embryos 48 h after BrdU injection (j,l; confocal stack analyse in n) is not observed in *Fgfr1^{fl/f};hGFAP^{Cre}* embryos (k,m; confocal stack analyses in o). LV, lateral ventricle; M, midline; GW, glial wedge; IG, indusium griseum. Scale bars: 100 μ m in a–d, 150 μ m in f,g,j and k, 75 μ m in h,i,l and m, 30 μ m in n and o. Error bars represent s.e.m.



hypothesis that *Fgfr1* may be important for the proper formation of midline glial structures and/or may secondarily affect the distribution of the chemotactic signals that they emanate. Furthermore, the presence of *Fgfr1* mRNA in the developing neocortex also suggests that FGFR1 may function within neurons fated to cross the midline. For example, FGFR1 might act as a receptor/coreceptor for midline guidance cues or may regulate the expression of receptors for known chemotactic signals.

To clarify the role of FGF signaling in commissure development, we investigated whether the targeted inactivation of *Fgfr1* in radial glial progenitors might result in neuronal or glial differentiation defects that could have an impact on axon guidance. The *Fgfr1^{fl/f};hGFAP^{Cre}* and *Fgfr1^{fl/f};Nes^{Cre}* mice appeared normal with respect to the differentiation of neurons and astroglial cells as shown by β III tubulin, calretinin and GFAP immunostaining (Fig. 1f–h and Supplementary Fig. 3 online). At E16.5, control and *Fgfr1^{fl/f};hGFAP^{Cre}* mice showed similar amounts of DCC, TAG-1/Cntn2, L1 and N-cadherin (Supplementary Fig. 3), proteins that are involved in commissural axon fasciculation and guidance. In the *Fgfr1* mutants, some of the DCC-positive axons reached the midline, but were less compactly organized and did not appear to cross it. Furthermore, the expression of *Slit2*, *Slit3*, *Robo1* and growth-associated protein 43 (*Gap43*) genes, whose mutations also result in commissural defects³², did not appear to be altered in *Fgfr1* mutant embryos (Supplementary Fig. 4 online). Therefore, we excluded perturbations in the expression levels of several axonal and glial factors necessary for midline guidance as a potential explanation for the observed phenotype in *Fgfr1* mutant mice. However, the expression of *Ntn1* appeared to be decreased in the indusium griseum of *Fgfr1^{fl/f};hGFAP^{Cre}* mice, while being maintained in the glial wedge and other regions (Supplementary Fig. 4). This could potentially be a consequence of the altered morphogenesis of astroglia in the indusium griseum.

Neuronal specific *Fgfr1* mutants lack commissure dysgenesis

To directly assess the potential contribution of FGFR1 signaling within neurons during commissure formation, we generated mice carrying a neuron-specific inactivation of the *Fgfr1* gene. We did so by crossing the *Fgfr1^{fl/f}* strain with mice bearing the *Syn1-Cre* transgene, to obtain *Fgfr1^{fl/f};Syn1^{Cre}* mutants. The *Syn1-Cre* transgene is specific to neurons and begins to be expressed at approximately E12.5 (ref. 33). Using the *Rosa 26R lacZ* reporter gene for Cre-mediated recombination³⁴, we

observed robust β -galactosidase (β -gal) staining in all cortical layers of *Fgfr1^{fl/f};Syn1^{Cre}* at P0 (Fig. 2a,b). Most of this cortical staining is presumed to be neuronal in nature as most of the cortical cells at P0 are neurons. At higher magnification, labeled fibers could be seen descending from the cortex into the white matter of *Fgfr1^{fl/f};Syn1^{Cre}* mice. This staining was identical to that obtained with heterozygous *Fgfr1^{fl/+};Syn1^{Cre}* littermates (data not shown). Hence, Cre recombination was widespread throughout the cerebral cortex.

Fgfr1^{fl/f};Syn1^{Cre} mice did not show any detectable differences in brain morphology or histological organization when compared to control littermates (Fig. 2c,d). Furthermore, *Fgfr1^{fl/f};Syn1^{Cre}* mice appeared to have normal commissures. This was confirmed with staining for TAG1 (Fig. 2e,f). Finally, midline glial structures were preserved in the *Fgfr1^{fl/f};Syn1^{Cre}* mice. These mice did not have any apparent defects in glial wedge, midline zipper or indusium griseum astroglia (Fig. 2g,h). Therefore, defects in the formation of the indusium griseum and the telencephalic commissures are specific to mutants with targeted inactivation of *Fgfr1* in radial glial progenitors, as they are not present in neuron-specific mutants of *Fgfr1*.

Fgfr1 is required for midline radial glia translocation

Fgfr1 loss of function was associated with a decrease in the number of GFAP⁺ cells in the apparent process of migrating toward the prospective indusium griseum area, as well as with the maintenance of radial glial cell processes in this region (Fig. 1f–h). To assess whether *Fgfr1^{fl/f};hGFAP^{Cre}* mice had defective migration of cells from the glial wedge to the indusium griseum, coronal cortical slices were prepared from E14.5 control and *Fgfr1^{fl/f};hGFAP^{Cre}* embryos and maintained *in vitro*. The fluorescent dye tracer PKH26 was applied to the dorso-medial ventricular zone, in order to label presumptive radial glial cells in the glial wedge (Fig. 3a,b). The movement of the cells in these explants was monitored by fluorescence microscopy over a 48-h period.

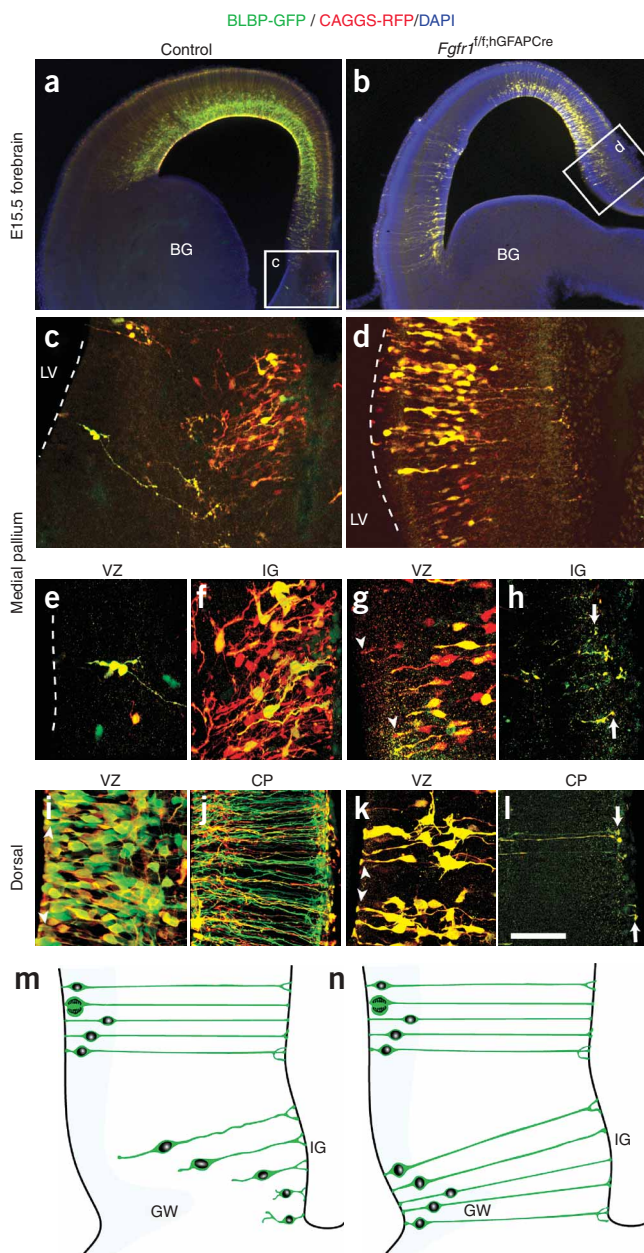


Figure 4 Midline radial glia translocation is absent in glial-specific *Fgfr1* mutant embryos. (a–l) Coronal sections of E15.5 control (a, c, e, f, i, j; $n = 4$) and *Fgfr1*^{fl/fl};hGFAPCre embryos (b, d, g, h, k, l; $n = 3$) embryos coelectroporated *in utero* at E14.5 with 4:1 of *Blbp-GFP* and *CAGGS-RFP* constructs. (c–l) Confocal z-stack (45- μ m) projections. In the control, numerous cell bodies of GFP-positive (GFP⁺) radial glial cells were present in the indusium griseum (IG; f) and the ventricular zone of the dorsal pallium (j), but not in the ventricular zone of the medial pallium (e). The apical endfeet were absent from GFP⁺ radial glial cells in the ventricular zone of the medial pallium (e) but not dorsal pallium (arrowheads in i). Basal processes extended to the pial surface in both locations (f, j). GFP⁺ radial glial cells in *Fgfr1*^{fl/fl};hGFAPCre mice had cell bodies in both the dorsal (k) and the medial (g) pallial ventricular zone with apical endfeet present at the ventricular zone surface (arrowheads in g, k) and basal processes extending to the pial surface (arrows in h, l). (m, n) Schematic model illustrating the translocation of midline radial glial cells from glial wedge to indusium griseum in control embryos (m) and its failure in *Fgfr1* mutants (n). Scale bars: 500 μ m in a and b, 100 μ m in c and d, 50 μ m in e–l.

Both control and *Fgfr1*^{fl/fl};hGFAPCre littermates had abundant BrdU labeling in the ventricular zone, including the glial wedge region, 1 h after a single BrdU injection at E14.5 (Fig. 3f–i). Very little BrdU labeling was visible in the cortical plate, except in the meninges. By E16.5, in control embryos many BrdU-positive (BrdU⁺) cells double-labeled with the astroglial marker GLAST were visible in the presumptive indusium griseum at the midline, as well as throughout the region between the glial wedge and the indusium griseum (Fig. 3j, l; magnified confocal images in Fig. 3n). A few BrdU⁺ cells that were GLAST-negative (GLAST⁻), presumably neurons, were also present in this region in E16.5 control embryos. In *Fgfr1*^{fl/fl};hGFAPCre littermates, the BrdU/GLAST double-labeled cells were absent in both the presumptive indusium griseum and the area between the glial wedge and the indusium griseum, whereas BrdU single-labeled cells were detectable in the cortical plate (Fig. 3k, m; magnified confocal image in Fig. 3o). Furthermore, an accumulation of GLAST-positive (GLAST⁺) cells was visible in the presumptive indusium griseum in control embryos (Fig. 3j, l, n) but not in *Fgfr1*^{fl/fl};hGFAPCre littermates (Fig. 3k, m, o). We detected no changes in radial glial cell proliferation in the glial wedge and adjacent dorsomedial ventricular zone in *Fgfr1*^{fl/fl};hGFAPCre mice. The density of BrdU⁺ was 6.5×10^{-4} (± 0.6) cells mm^{-3} in controls versus 7.8×10^{-4} (± 0.4) cells mm^{-3} in *Fgfr1*^{fl/fl};hGFAPCre mice (mean (\pm s.e.m.); $P = 0.16$, Student's two-tailed *t*-test). Combined, these data suggest that a population of radial glial cells born at E14.5 migrated from the nearby ventricular zone to the presumptive indusium griseum in control mice, but not in *Fgfr1* mutant littermates.

We next investigated whether the radial glial cells in the glial wedge migrate to the cortical plate by somal translocation. Somal translocation requires the nascent astrocyte to detach its ventricular (apical) endfoot while translocating its cell body by shortening the pial process^{1,3}. To selectively label radial glial cells, we used a vector expressing the enhanced green fluorescent protein (GFP) under the BLBP radial glial promoter (BLBP-GFP). This vector was electroporated in the dorsomedial ventricular zone of E14.5 wild-type (Fig. 4a) or *Fgfr1*^{fl/fl};hGFAPCre (Fig. 4b) mouse embryos, together with a control vector expressing the red fluorescent protein under the ubiquitous chicken β -actin promoter (CAGGS-RFP). The embryos were harvested 24 h later, and the fate of GFP-labeled radial glial cells was assessed by confocal microscopy (Fig. 4c–l). In this experiment, radial glial cells expressed both the BLBP-GFP and the CAGGS-RFP vectors, and thus appeared yellow; non-radial glial cells expressed the CAGGS-RFP vector only, and thus appeared red. In control embryos ($n = 4$), over the E14.5–E15.5 span, radial glia in the whole dorsal telencephalon with

By 24 h, labeled cells had reached the midline pial membrane in control embryos (arrowheads in Fig. 3c). In cortical slices prepared from *Fgfr1*^{fl/fl};hGFAPCre embryos, however, we observed little or no cell migration away from the ventricular zone, and no label accumulated in the indusium griseum area (Fig. 3d). The average distance of migration of midline cells in *Fgfr1*^{fl/fl};hGFAPCre embryos was less than half of that achieved in controls ($n = 7$ control and $n = 6$ *Fgfr1*^{fl/fl};hGFAPCre embryos; Fig. 3e). Labeled cells reached the pia in 4 of 7 explants in control mice, but in none of the explants prepared from *Fgfr1*^{fl/fl};hGFAPCre mice. These data indicate that *Fgfr1* is required for the migration of cells from the ventricular zone to the subpial region of the dorsomedial pallium.

These experiments, however, did not distinguish whether these migrating cells corresponded to the astroglial cells of the indusium griseum. Most indusium griseum cells are born around E14.5 (ref. 4). Hence, we labeled dividing cells at E14.5 by *in vivo* 5-bromodeoxyuridine (BrdU) incorporation and traced their location and fate in the medial pallium of both control and *Fgfr1* mutant embryos (Fig. 3f–o).

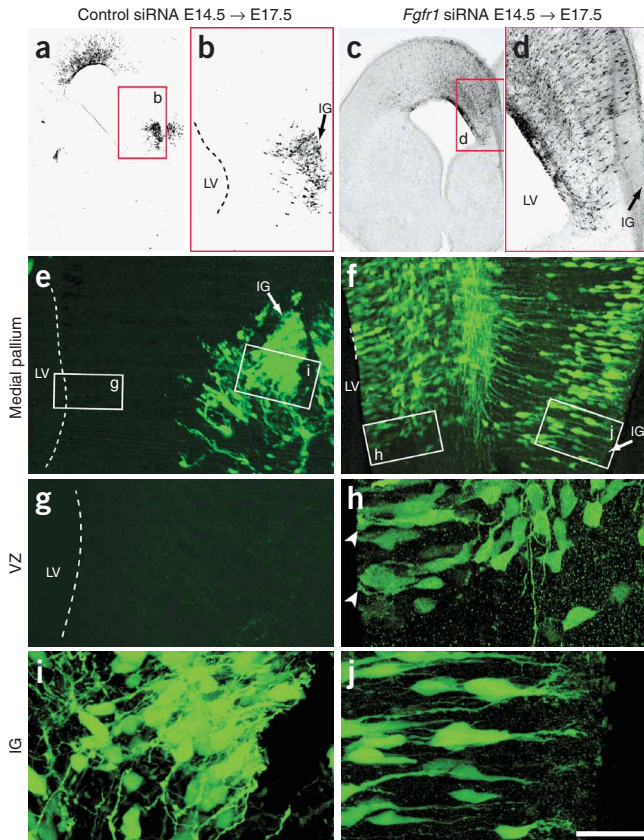


Figure 5 Cell-autonomous regulation of midline radial glia translocation by FGF signaling. (a–j) Coronal sections of E17.5 embryos electroporated *in utero* at E14.5 with pCGLH vectors expressing control shRNAs (a,b,e,g,i; $n = 7$ point-mutated and $n = 5$ empty shRNA vector) or *Fgfr1* shRNAs (c,d,f,h,j; $n = 7$). Anti-GFP diaminobenzidine immunohistochemistry (a–d) and fluorescence (e–j) in electroporated brains revealed that dorsomedial ventricular zone cells expressing control shRNAs (a,b,e,g,i) but not *Fgfr1* shRNAs (c,d,f,h,j) migrated to the indusium griseum (IG). Numerous GFP⁺ cells with bipolar morphology and apical endfeet (arrowheads) remained in the dorsomedial ventricular zone when expressing *Fgfr1* shRNAs (h compared to control in g). In contrast, many GFP⁺ cells in the dorsal pallium remained in the ventricular zone irrespective of electroporation with control or *Fgfr1* shRNAs. Images in g,i and h,j are high magnifications of the respective boxed areas shown in e and f. Panels b and d are high magnification of red boxes in panels a and c. Scale bars: 600 μm in a and c, 100 μm in e and f, 30 μm in g–j.

Cell-autonomous regulation of glial translocation by FGFR1

To further understand whether FGFR1 signaling within midline radial glial cells is required for their translocation, we performed an *in vivo* knockdown of *Fgfr1* mRNA by electroporating radial glial cells *in utero* with pCGLH vectors expressing either small-hairpin RNA (shRNA) targeting the *Fgfr1* ($n = 7$), control shRNA with four point mutations in the *Fgfr1* target sequence ($n = 7$) or empty shRNA vectors ($n = 5$). The shRNA targeting *Fgfr1* resulted in decreased *Fgfr1* expression (Supplementary Fig. 5 online). All pCGLH vectors coexpressed shRNA and GFP, which allowed us to directly visualize the behavior of the transfected cells in the wild-type background. Electroporation of control shRNA harboring four mutations with respect to the target RNAi sequence or electroporation of the empty shRNA vector produced the same phenotype previously observed after electroporating the BLBP-GFP vector in control embryos (Fig. 4a,c): 3 d after transfection, cells had already left the medial ventricular zone and densely populated the subpial region in the prospective indusium griseum area (Fig. 5a,b). No radial glial endfeet or cell bodies could be visualized in the dorsomedial ventricular zone (Fig. 5b), suggesting that these radial glial cells had left behind no progeny. Transfected cells in the dorsal telencephalon remained in the ventricular zone (Fig. 5a), further demonstrating that these different populations of radial glial cells translocate to the upper layers according to completely different schedules. Notably, radial glial cells transfected with *Fgfr1* shRNA did not leave the dorsomedial ventricular zone (Fig. 5c,d). At higher magnification (Fig. 5e–j), it was clear that whereas midline radial glial cells electroporated with control vector left the ventricular zone and accumulated in the indusium griseum (Fig. 5e–i), midline radial glial cells harboring a knockdown of *Fgfr1* mRNA could not undergo their early translocation toward the indusium griseum prospective region and behaved similarly to all the other radial glial cells (Fig. 5f,h). Further, midline radial glia left no endfeet in the ventricular zone (Fig. 5g), whereas many radial glial cell endfeet were attached to the ventricular surface in radial glial cells transfected with *Fgfr1* shRNA (arrowheads in Fig. 5h). Because all the surrounding cells had normal *Fgfr1* expression, the data demonstrate that *Fgfr1* is directly required within the translocating cells and is not secondarily affecting them through cell-to-cell interactions. Notably, cells with an *Fgfr1* mRNA knockdown could reach the dorsomedial cortical plate 3 d after electroporation, but appeared to have neuronal morphology identical to that of other cortical plate areas (Fig. 5j), suggesting that the disruption of *Fgfr1* does not alter neuronal migration.

FGFs are sufficient to induce radial glial translocation

Our *in situ* hybridization data show that endogenous *Fgf8* and *Fgfr1* messages are restricted to the midline at the same time and place at

the exception of the medial region were bipolar, with their apical process firmly attached to the ventricular basement membrane (Fig. 4a,i,j). In the medial region of the pallium, however, the GFP-labeled radial glial cells had already detached their apical endfeet from the ventricular zone (Fig. 4a,c,e), and most had already settled in the prospective indusium griseum (Fig. 4c,f) while a few were still visible en route to this area (Fig. 4c,e). Notably, astroglial cells were seen pulling themselves up by their intact basal process attached to the prospective indusium griseum area (Fig. 4c,e).

To understand whether this cell movement was disrupted in the *Fgfr1* mutants, we electroporated these constructs in *Fgfr1^{fl/fl}hGFAP^{Cre}* embryos ($n = 3$). Notably, radial glial cell bodies throughout the telencephalon remained in the ventricular zone with their apical endfeet attached to the ventricular basement membrane in *Fgfr1* mutants (Fig. 4b,d). In the medial pallial region, GFP-labeled radial glial cells were attached by their apical endfeet to the lateral ventricle (Fig. 4g), and no labeled cell populated the indusium griseum primordium (Fig. 4h), in marked contrast to what was observed in controls. Radial glial morphology in the dorsal pallium of *Fgfr1* mutants (Fig. 4k,l) resembled that of wild-type embryos (Fig. 4i,j). These experiments illustrate the early detachment of radial glia apical processes from the dorsomedial ventricular zone and their somal translocation from the ventricular zone to the indusium griseum primordium at E14.5–E15.5, a time when upper layer cortical neurons are generated in the ventricular zone of the cerebral cortex (schematic drawing in Fig. 4m). Furthermore, this process did not occur when FGFR1 signaling was disrupted in these cells (Fig. 4n). Although the detachment and translocation process could be simply delayed in these mutants, the absence of indusium griseum astroglia at P0 (Fig. 1f–h) argues against this notion.

which the indusium griseum astroglia are migrating. We therefore tested whether the exogenous application of FGF8 protein to an area of the cortical plate that normally has little or no expression of *FGF8* and *Fgfr1* is capable of inducing the migration of cells from the ventricular zone to the cortical plate. Cell migration was detected using the vital dye PKH26 applied to the dorsolateral ventricular zone of cortical slices, after a bead soaked in FGF8 or control bovine serum albumin (BSA) was implanted into the dorsal cortical plate (Fig. 6a,b). Numerous cells were visible in the intermediate zone and cortical plate in the area adjacent to the FGF8 bead 24 h after dye application (Fig. 6b). These cells appeared to be moving directly up to the cortical plate in alignment with radial glial fibers. In comparison, the implantation of BSA-soaked beads did not have any effect (Fig. 6a).

We further investigated whether FGF protein gradients stimulated neuronal or glial cell translocation in explants of whole E13.5 dorsal cortex. After FGF or BSA bead implantation and a 48-h culture period, explants were sectioned and immunostained with various cell markers. Dorsal cortices embedded with control beads showed the expected organization into ventricular zone, intermediate zone and cortical plate. The ventricular zone contained tightly associated cell bodies of the radial glial cells. In contrast, in dorsal cortices embedded with FGF2 or FGF8 beads, radial glial cells were displaced toward the cortical plate. This displacement was demonstrated by double immunolabeling of the proliferating radial glial cell somata with the cell cycle markers PCNA and BLBP (Fig. 6c,d) or BLBP and RC2 (Fig. 6e,f). There was a dearth of immunostained radial glial apical projections in the ventricular zone layer (compare Fig. 6c with Fig. 6d), suggesting that these cells had detached their apical process from the ventricular zone. Notably, GFAP-immunoreactive cells were not present in control explants (Fig. 6g) and were only present in FGF-treated explants in the uppermost region of the explants (white arrows in Fig. 6h).

To confirm that FGFs induced an upward movement of radial glial cells, we pulse-labeled the explants with BrdU at the beginning of culture. After 48 h, most BrdU-labeled nuclei in control cortices remained within the ventricular zone (Fig. 6i). In contrast, dorsal cortices embedded with either FGF2 or FGF8 beads showed a dispersion of BrdU-labeled nuclei within the explant and a heavy accumulation at the pia (Fig. 6j). Most of the BrdU⁺ cells displaced in the upper layers extended RC2-positive (RC2⁺) fibers consistent with a radial glia

phenotype (arrowheads in Fig. 6j inset). These data suggest that the BrdU-labeled cells in these areas comprise both the cells coming from the ventricular zone, which were initially labeled by BrdU, and their offspring after cell division.

Proliferating radial glial cells were quantified in different areas of the explants 48 h after bead implantation. In comparison to BSA, FGF2 and FGF8 induced a 5.9-fold and a 2.9-fold increase, respectively, in the density of PCNA-positive (PCNA⁺) cells in the cortical plate and intermediate zone, whereas neither factor caused a change in

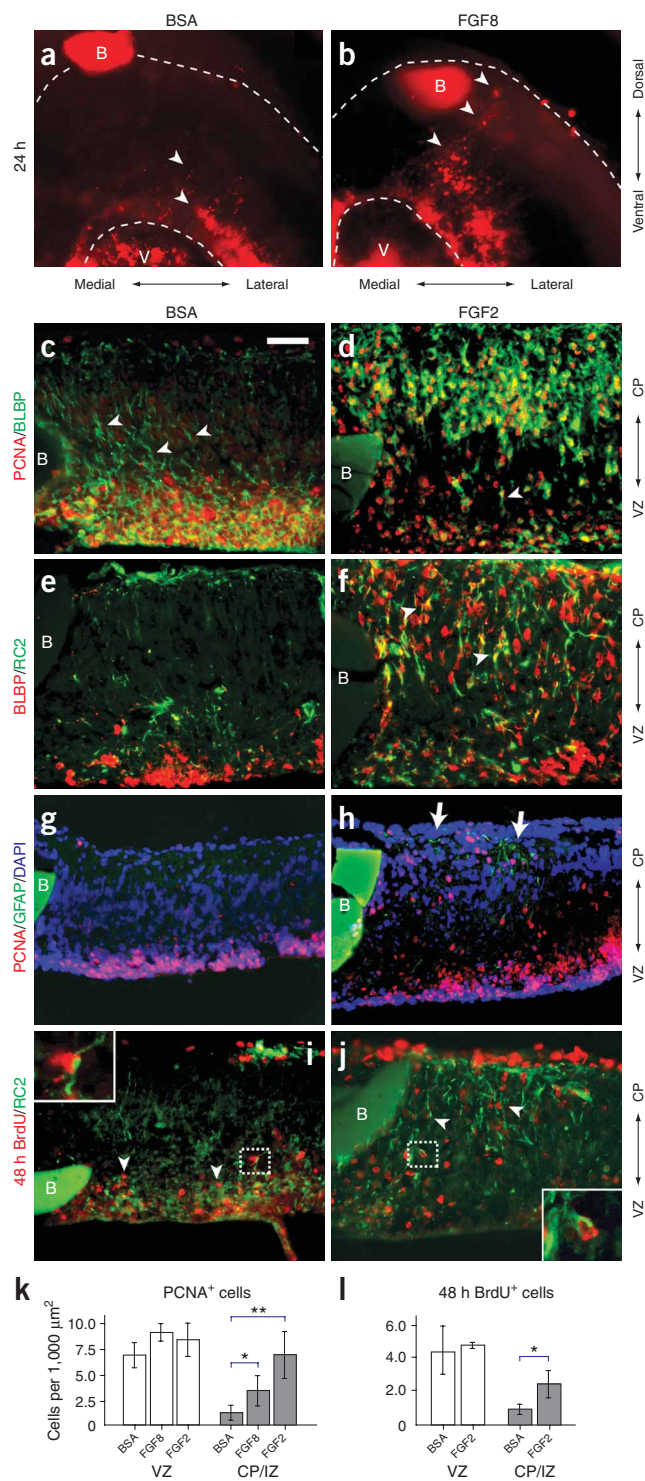


Figure 6 FGF signaling is sufficient to induce premature radial glial cell translocation in developing cortex. (a,b) Coronal slices of wild-type E14.5 mouse telencephalon 24 h after implantation in the dorsolateral cortical plate with beads ('B') soaked in either BSA (a; $n = 5$) or FGF8 (b; $n = 4$) and labeled with PKH26 in the adjacent ventricular zone. In FGF8-treated explants, cells migrated radially to the area adjacent to the bead (arrowheads). Scale bar, 100 μm . (c–j) Sections from E14.5 dorsal cortical explants implanted with BSA-soaked beads (c,e,g,i) or beads soaked in FGF2 protein (d,f,h,j) and cultured for 48 h. (c,d) PCNA/BLBP double immunostaining. (e,f) BLBP/RC2 double immunostaining. (g,h) GFAP/PCNA immunostaining with DAPI counterstaining, showing GFAP-immunoreactive cells in the cortical plate of FGF2-treated explants (arrows in h). (i,j) Proliferating cells pulse-labeled with BrdU at the beginning of FGF bead application were analyzed after 48 h by anti-BrdU immunohistochemistry. BrdU⁺ cells in both control and FGF2-treated explants had RC2⁺ fibers (arrowheads in i,j; insets show 3 \times magnification). CP, cortical plate; V, ventricle; VZ, ventricular zone. Scale bar, 50 μm . (k,l) Quantification of PCNA⁺ and BrdU pulse-labeled cells (48 h BrdU⁺) in two bins of tissue adjacent to the bead ($n = 4$ independent experiments). Both BrdU⁺ and PCNA⁺ cell densities were increased by treatment with FGF2 and FGF8 as compared to BSA in the cortical plate and intermediate zone. * $P = 0.05$ and ** $P < 0.001$, one-tailed Student's t -test. Error bars represent s.e.m.

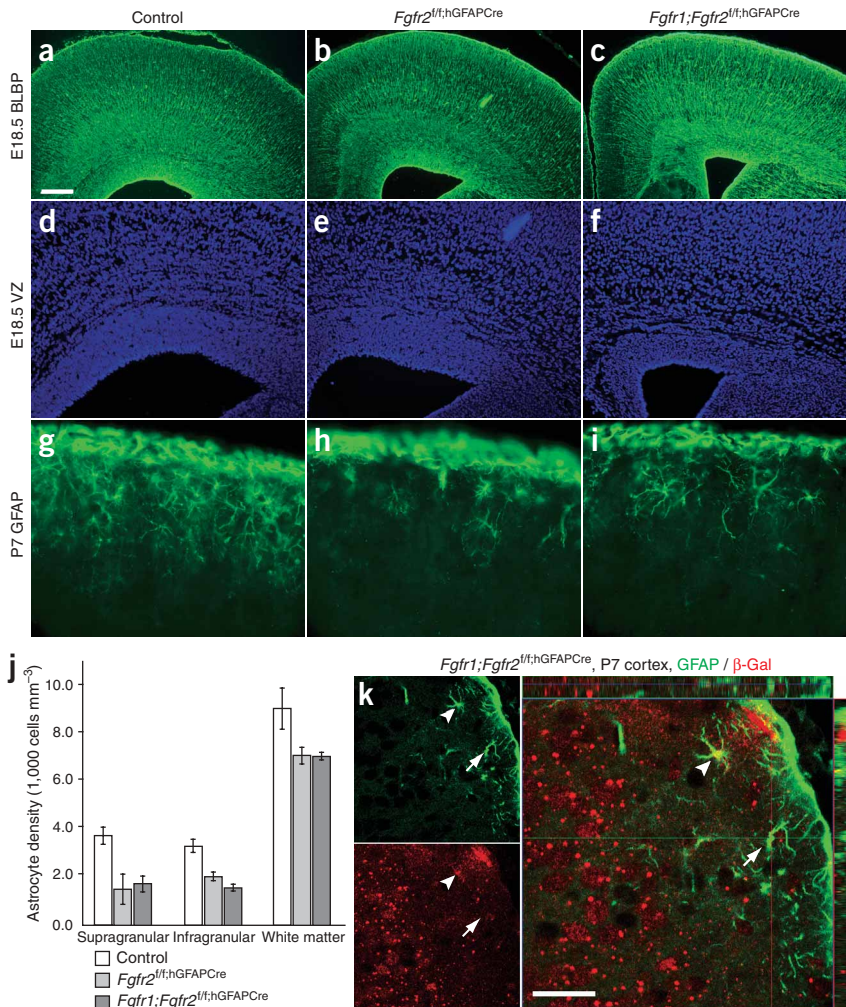


Figure 7 *Fgfr2* is required for astroglial targeting to the dorsolateral cortex (**a–c**) BLBP staining in control (**a**), *Fgfr2*^{fl/fl};hGFAPCre (**b**) and *Fgfr1*; *Fgfr2*^{fl/fl};hGFAPCre (**c**) E18.5 embryos, showing normal radial glial morphology in *Fgfr2* single and *Fgfr1*/*Fgfr2* double mutant mice. (**d–f**) DAPI staining in E18.5 control (**d**), *Fgfr2*^{fl/fl};hGFAPCre (**e**) and *Fgfr1*; *Fgfr2*^{fl/fl};hGFAPCre (**f**) embryos, showing normally arranged and densely packed nuclei in the ventricular zone of *Fgfr2* and *Fgfr1*/*Fgfr2* mutant embryos. (**g–j**) GFAP staining in the cortical plate of control (**g**), *Fgfr2*^{fl/fl};hGFAPCre (**h**) and *Fgfr1*; *Fgfr2*^{fl/fl};hGFAPCre (**i**) mice at P7. (**j**) Density of GFAP⁺ cells in the supragranular and infragranular dorsolateral cortex and subcortical white matter. The *Fgfr2* and *Fgfr1*/*Fgfr2* mutant mice differed significantly from controls in the density of GFAP⁺ cells in the supragranular layer ($P = 0.005$), infragranular layer ($P = 0.05$) and white matter ($P = 0.009$) (ANOVA using Scheffé *post-hoc* tests). (**k**) Confocal images of GFAP and β -gal (reporter) double immunostaining in *Fgfr1*; *Fgfr2*^{fl/fl};hGFAPCre mice. Arrowhead, double-labeled cell; arrow, GFAP⁺ astrocyte that failed to show β -gal reporter expression. Scale bars: 100 μ m in **a–c**, 50 μ m in **d–f**, 25 μ m in **g–i**, 12.5 μ m in **k**. Error bars represent s.e.m.

PCNA⁺ cells in the ventricular zone area (Fig. 6k). Furthermore, the density of BrdU⁺ cells 48 h after pulse labeling increased by 2.5-fold in the cortical plate and intermediate zone after FGF2 treatment (Fig. 6l). These data illustrate that exogenous FGFs emanating from the bead elicited an increase in number of radial glial cells, probably due to their well-known mitogenic effect. In addition, FGFs are sufficient to induce a premature upward movement of radial glial cells. Cells did not show a chemotropic movement toward the bead, but rather translocated their cell bodies in a radial fashion toward the cortical plate. This is consistent with the idea that they were not free to move within the tissue but were ‘pulled up’ by their pial processes.

FGFR2 regulates astrocyte targeting to dorsolateral cortex

Whereas *Fgfr1* mRNA is expressed in a gradient peaking at the dorsomedial ventricular zone and indusium griseum, the *Fgfr2* message is enriched in the ventricular zone and cortical plate of the dorsolateral cortex during mid- and late embryogenesis^{21,22,35}. To investigate whether *Fgfr2* has a role in astroglial somal translocation that normally occurs in the cerebral cortex at the end of gestation, we generated mice lacking functional *Fgfr2* in radial glia by *hGFAP-Cre*-mediated recombination of *Fgfr2*^{fl/fl} alleles³⁶; we intercrossed these mice with *Fgfr1*^{fl/fl};hGFAPCre to generate *Fgfr1*; *Fgfr2*^{fl/fl};hGFAPCre double mutant mice. Both the *Fgfr2*^{fl/fl};hGFAPCre and *Fgfr1*; *Fgfr2*^{fl/fl};hGFAPCre double mutants were viable and fertile and demonstrated a decrease in the *Fgfr2* message by semiquantitative real-time reverse transcriptase-

polymerase chain reaction (RT-PCR; **Supplementary Fig. 5**). Similarly to the *Fgfr1*^{fl/fl};hGFAPCre mice, *Fgfr2*^{fl/fl};hGFAPCre mice showed a subtle reduction in cortical size compared to control mice (Fig. 7a,b), which was accentuated in the double mutant mice (Fig. 7a,c). Furthermore, the thickness of the ventricular zone was not affected in *Fgfr2*^{fl/fl};hGFAPCre mice, although it appeared to be reduced in *Fgfr1*/*Fgfr2* double mutant mice (Fig. 7d–f), consistent with the previously documented role of *Fgfr1* and *Fgfr2* in radial glial cell proliferation^{22,23}. In both *Fgfr2*^{fl/fl};hGFAPCre single and *Fgfr1*; *Fgfr2*^{fl/fl};hGFAPCre double mutant mice, we did not observe any abnormalities in the morphology or distribution of radial glial cells at embryonic stages of development. In particular, radial glial cells had densely packed cell bodies in the ventricular zone and extended regularly arrayed processes to the pial layer, as assessed by BLBP and RC2 immunostaining at E18.5 (Fig. 7a–c and data not shown). Despite the lack of apparent abnormalities in the radial glia of late gestation embryos, there was a decreased density in GFAP⁺ astrocytes within the dorsal cortex in both single and double mutant mice at P7 (Fig. 7g–i). Unbiased counting confirmed that the number of astroglia that reached the cortex in *Fgfr2*^{fl/fl};hGFAPCre ($n = 3$) and *Fgfr1*; *Fgfr2*^{fl/fl};hGFAPCre ($n = 3$) mice was significantly reduced ($F_{1,23} = 25$; $P < 0.0001$) compared to that in Cre-negative (Cre⁻) control mice at P7 ($n = 4$). Moreover, the severity of this reduction was similar in *Fgfr1*/*Fgfr2* double mutant and *Fgfr2* single mutant mice, suggesting that *Fgfr2* had a major role (Fig. 7j). In *Fgfr2*^{fl/fl};hGFAPCre mice, the greatest loss of astrocytes was observed in the upper cortical layers (60% decrease), and the smallest loss was in the subcortical white matter (22% decrease); an intermediate reduction in astrocyte density was seen in the inferior cortical layers (39% decrease). The fact that the loss of GFAP⁺ astrocytes became increasingly severe with greater distance from the subventricular zone is consistent with a role for *Fgfr2* in astrocyte displacement from the ventricular zone to the cortex. Double staining for GFAP and the Cre reporter gene β -gal in

Fgfr2 knockout mice revealed that only a portion of the GFAP⁺ astrocytes found in the cerebral cortex were reporter-positive (Fig. 7k). This heterogeneity implies that some of the astrocytes that were able to translocate to the cortex in *Fgfr2* mutant mice might have escaped Cre recombination.

DISCUSSION

We showed that radial glial cells in the dorsomedial ventricular zone detach their apical processes at midneurogenesis to translocate to the pia, where they contribute to form the indusium griseum at the cortical anterior midline. These midline glial cells are born concurrently with neurons, contradicting the common belief that neurons must be born first, followed by glial cells. Loss-of-function mouse models, shRNA knockdown and gain-of-function experiments demonstrated that the *Fgfr1* gene is essential for the translocation of these radial glial cells to the medial pallium (schematic in Fig. 4m,n). FGFR1 is likely to act by binding FGF8 and other ligands that are enriched in this region. We suggest that a failure of this mechanism is a causative factor in the callosal dysgenesis present in *Fgfr1* mutant mice. By contrast to the midline regions, radial glia in lateral regions of the cerebral cortex undergo somal translocation only at the end of neurogenesis. This process is disrupted when the *Fgfr2* gene is excised in radial glial cells.

The differentiation of astroglial cells in the dorsomedial pallium begins much earlier than that of other cortical astrocytes, as midline glial cells have largely completed their migration to the indusium griseum by E17.5, a time when other cortical astroglia are still anchored at the ventricular zone. It has been shown that mechanical or genetic disruptions of midline glial cell morphogenesis result in acallosal phenotypes^{6–8}, strongly suggesting that these cells must be properly positioned when commissural axons begin crossing the midline. We showed that inactivating *Fgfr1* in radial glial cells produces a specific disruption of the corpus callosum and hippocampal commissure that does not reflect a general defect in neurite outgrowth. The mice harboring *Fgfr1* mutations lacked the indusium griseum, but had no impairments in the formation of the glial wedge or midline zipper. We suggest that the specific lack of the indusium griseum may be the primary cause of disrupted commissure development.

Our results suggest that the failure in the formation of the indusium griseum is attributable to a role for *Fgfr1* in the translocation of radial glial cells from the dorsomedial ventricular zone (glial wedge region) to the subpial region of the dorsomedial pallium. This interpretation is supported by multiple lines of evidence. First, targeting an *Fgfr1* mutation to radial glial cells produced a loss of GFAP⁺ cells in the indusium griseum or in transit from the glial wedge region to the indusium griseum, but not in the glial wedge. This suggests that the FGFR1-deficient radial glial progenitors of the glial wedge can differentiate into GFAP⁺ cells but cannot migrate out from this region. This defect was not seen in mice with a disruption of *Fgfr1* in neurons, suggesting that *Fgfr1* is required in glia to mediate these effects. Second, in *Fgfr1* mutant mice, astroglial cells born in the ventricular zone at E14.5 did not migrate in the prospective indusium griseum. Hence, the indusium griseum does not form *in situ* but arises, as suggested here, by an FGF-dependent migration of astroglia into the midline pallium. Third, there is active movement of cells from the dorsomedial ventricular zone toward the presumptive indusium griseum at E14.5, and targeting the *Fgfr1* mutation to radial glial cells impaired this movement, suggesting that FGF signaling is critical for cell migration. Marking ventricular zone radial glial cells *in vivo* by a GFP construct driven by a radial glial promoter showed that a population of radial glial cells at the dorsal midline detached their apical processes from the ventricular zone and pulled themselves up to the subpial layer in the

prospective indusium griseum. These midline radial glial cells were unlike all the other cortical radial glial cells in that they appeared to have left no daughters in the ventricular zone (schematic outline in Fig. 4m). This early detachment of dorsomedial radial glial cells was not observed in glial-specific *Fgfr1* mutant mice.

The dorsomedial cortical wall is an FGF signaling center. We and others³⁰ have shown that *Fgf8*, *Fgf17* and *Fgf18* mRNAs are expressed at E14.5 in the glial wedge and nascent indusium griseum. *Fgf8* hypomorphic mice have defects in corpus callosum formation^{37,38}, and the inactivation of the *Fgf8* gene in zebrafish results in commissural defects³⁹. Therefore, these FGF sources near the midline may signal to nearby radial glial cells via *Fgfr1* expressed in the latter. Consistent with this, at stages of development when callosal connections begin to form, active FGFR signaling as detected by *Spry1* is enriched in the glial wedge and is drastically reduced in glial-specific *Fgfr1* mutants.

The role of *Fgfr1* in directing somal translocation is both cell type-specific (that is, restricted to astroglia) and cell-autonomous (that is, independent from cell-to-cell communication). Neuronal migration did not seem to be affected by the knockdown of *Fgfr1* mRNA and the loss of FGFR1 in neurons did not produce cortical laminar defects. Furthermore, cells harboring shRNA-mediated knockdown of *Fgfr1* mRNA were unable to translocate to the prospective indusium griseum in brains where other surrounding cells expressed the wild-type *Fgfr1* gene product. Hence, *Fgfr1* is required in radial glia and, according to the hypothesis presented here, regulates their detachment from the ventricular zone to migrate subpially in response to gradients of FGFs.

We suggest that the failure of this translocation process is responsible for the dysgenesis of the dorsal telencephalic commissures. This is supported by the close correlation noted in our series of mutants between midline glial defects and the extent to which the formation of the callosum is disrupted. Incidentally, this is consistent with the persistence of normal ventral commissures in *Fgfr1* mutants, as these areas are not enriched in *Fgfr1* expression and do not show abnormal glial positioning in the *Fgfr1* mutant mice. Notably, the *Drosophila* FGFR homolog *breathless* is also involved in midline glial cell migration and commissure formation in the CNS (ref. 40). In *Fgfr1* mutant flies, posterior midline glial cells (MGP cells) are produced properly but their migration is defective and they remain in their original segments. The dislocation of MGP leads to abnormal arrangement of commissural axons. Hence, the role of FGF receptors in glial cell positioning and commissure development is evolutionarily conserved.

Although FGF signaling has been implicated in neurite outgrowth and axon guidance^{41,42}; the selective inactivation of *Fgfr1* in neurons did not produce any detectable phenotype. It is possible that some of the neurons escaped *Fgfr1* inactivation; however, no intermediate phenotype was observed in the *Fgfr1^{fl/ESyn1}Cre* mice, although the other models clearly demonstrate that they are possible. The normal formation of midline glial structures in the neuron-specific *Fgfr1* mutants demonstrates that the glial defects are not secondary to a primary requirement for *Fgfr1* in neurons.

The question remains as to the mechanism by which glia of the indusium griseum promote axon guidance at the dorsal telencephalic midline. In the mouse, the first cortical axons to cross are those of the anterior cingulate cortex at E15.5 (ref. 28,43), directly underneath the cells of the indusium griseum. The malpositioning of these cells may prevent them from expressing a callosal chemoattractant such as netrin-1. It is also possible that the persistence of radial fibers in the mutants represents a mechanical obstacle or a source of chemorepellent factors in front of the early callosal axon path.

Notably, both FGF2 and FGF8 are sufficient for inducing the premature translocation of actively proliferating radial glial cells in

embryonic explants of dorsal cortex. These cells did not appear to be moving toward the FGF gradient, but rather were directed radially toward the pial surface, suggesting a process of soma translocation rather than chemotropic attraction. Because all radial glia seem to be capable of responding to FGF stimulation, the circumscribed expression of FGFs to the midline presumably restricts radial glial detachment to a restricted area of the ventricular zone at midneurogenesis. Eventually, some other mechanism(s) must trigger the widespread radial glial cell translocation to the cerebral cortex after birth. Although a complete examination of the factors involved in this phenomenon is beyond the scope of this paper, our evidence implicates *Fgfr2*, but not *Fgfr1*, in radial glial cell translocation targeting the dorsolateral cerebral cortex. In the cerebral cortex of *Fgfr2* mutant mice GFAP⁺ cells were decreased despite the absence of any disruption in the morphology of radial glial cells during late embryogenesis. The deletion of *Fgfr2* caused a 60% decrease in cortical astrocytes at P7, in the absence of a substantial decrease in the thickness of the ventricular zone. Astrocyte density was decreased by only 20% in white matter, arguing against a primary defect in the differentiation of astroglial cells in these *Fgfr2* mutant mice. Considering the close homology in signal transduction among FGFR1 and FGFR2, these data are consistent with the idea that *Fgfr2* is involved in the translocation of astroglia from the ventricular zone to the cerebral cortex. More studies are required to understand the specific ligands that trigger this process at the appropriate time, and their provenance.

FGF2 and FGF receptors have a role in the proliferation of cortical and hippocampal progenitors^{16,44,45}. FGF2 and FGFR2 are also involved in the maintenance of radial glial cell fates, presumably by repressing neuronal differentiation^{22,46}. However, in agreement with previous data⁴⁷, *Fgfr1* mutants did not reveal any defects in proliferation or differentiation in the cerebral cortex, as assessed by BrdU incorporation and phenotypic analyses using astroglial (GLAST, GFAP and Slit2) or neuronal (TAG-1, neuropilin-1, Gap43, β III tubulin and calretinin) markers. Furthermore, the disruption of the *Fgfr1* gene in *Fgfr1*^{fl/fl};NesCre and *Fgfr1*^{fl/fl};GFAPCre mice did not lead to a substantial abnormality in either brain morphology or patterning, as assessed by *Pax6*, *Titf1*, *Foxg1*, *Lhx2/5* or *Pou3f1* gene expression (ref. 23 and data not shown). We conclude that *Fgfr1* has a role in radial glial cell proliferation in the hippocampal primordium²³, but this receptor does not seem to mediate the actions of FGF2 in cortical development. Although the FGFR2 gene product could, in principle, compensate for the lack of FGFR1, our initial results with *Fgfr2*^{fl/fl};GFAPCre mice and FGFR1;FGFR2^{fl/fl};GFAPCre double mutant mice show normal radial glial morphology and relatively mild defects in total brain size at the stages of development examined.

Later in development, FGF2 enhances the competence of cortical progenitors to respond to astroglial differentiation signals, allowing their transition into astrocytes^{11,12,22,46}. Consistent with these notions, the earliest differentiation of cortical astroglia occurs in the midline region, which strongly expresses FGFs and downstream signaling molecules. The inactivation of *Fgfr1* or *Fgfr2*, however, did not preclude progenitor cells from acquiring astrocyte fates, but prevented their early translocation to the pia. Hence, it can be hypothesized that not FGFR1/FGFR2 directly, but possibly other FGF-regulated molecules may be involved in the fate switch from neuronal to astrocyte progenitors.

METHODS

Mice. The genetically modified mouse lines *Tg(GFAP-Cre)25Mes*, *Fgfr1*^{fl/fl}, *Fgfr2*^{fl/fl}, *Tg(Nes-Cre)* and *Tg(SynI-Cre)* and mating strategies have been previously described^{23,25,27,33,48}. All experimental procedures involving mice were performed in accordance with the policies of the Yale Institutional Animal Care and Use Committee.

Commissure measurements. Three areas were chosen using landmarks within cresyl violet-stained coronal sections from *Fgfr1*^{fl/fl};GFAPCre ($n = 15$), *Fgfr1*^{fl/fl};NesCre ($n = 5$) and littermate controls ($n = 17$). Scale bars were used to measure the commissural white matter. The areas (Fig. 1d) corresponded to the corpus callosum, nucleus accumbens, and beginning of the anterior commissure (A), the dorsal fornix and fimbria (M), and the rostral hippocampus, hippocampal commissure and the medial habenular nucleus (P).

Axonal tracing. BDA (10,000 M_w , Molecular Probes) was injected with a stereotaxic surgery restraint system equipped with a nanoinjector (Stoelting; details in **Supplementary Methods** online). BDA was detected with avidin-conjugated horseradish peroxidase (avidin-HRP) and diaminobenzidine (DAB, Vector Labs) or fluorescein isothiocyanate-conjugated avidin DCS (FITC-avidin DCS, Vector Labs). For tracing with 1,1'-diiodo-3,3',3',3'-tetramethylindocarbocyanine perchlorate (DiI) and 4-(4-(dihexadecylamino)styryl)-N-methylpyridinium iodide (DiA) (Molecular Probes), neonatal mice (P0–P1) were killed by intracardial perfusion and postfixed in 4% paraformaldehyde (PFA). DiI- or DiA-coated hand-pulled glass pipette tips were implanted into the anterior cingulate, somatosensory cortex or hippocampus.

In utero electroporation and RNAi. For *in utero* gene transfer by electroporation, 1–2 μ l of DNA solution (4 mg ml⁻¹) was injected into the lateral ventricle and electroporated as previously described⁴⁹ (**Supplementary Methods**). For RNA interference experiments, a template for short-hairpin RNA (shRNA) synthesis was made by annealing a pair of oligonucleotides representing the sense and antisense strands of the *Fgfr1* target sequences into pCGLH shRNA vector coexpressing GFP. Mutated (four mutations per sequence) *Fgfr1* targeting sequences were used as a control (oligonucleotides sequences in **Supplementary Methods**). Equal amounts of three shRNA vectors targeting the *Fgfr1* gene or of three control vectors with mutated shRNA sequences were injected. An empty pCGLH shRNA vector coexpressing GFP was injected as an additional control in separate experiments. Fluorescent images were obtained using a Zeiss LSM500 confocal microscope. In selected cases, GFP was visualized using DAB immunohistochemistry with an antibody to GFP (anti-GFP, 1:3,000; A11122, Molecular Probes). The plasmid containing GFP driven by the mouse Fabp7 promoter (pBLBP-GFP) and the *CAGGS-RFP* plasmid have been previously described⁵⁰.

In situ hybridization and immunohistochemistry. Digoxigenin-labeled RNA probes were synthesized from cDNAs by *in vitro* transcription (Digoxigenin RNA labeling kit, SP6/T7, Roche) using previously described techniques¹⁶. Primary antibodies for immunohistochemistry were detected with Alexa-conjugated fluorescent secondary antibodies (Molecular Probes). For nonfluorescent detection, we used biotinylated goat anti-rabbit or goat anti-mouse antibodies (Vector Labs) followed by avidin-HRP and DAB detection (Vector Labs). For the analyses of cell proliferation and lineage tracing, BrdU was injected (50 μ g g⁻¹, i.p.) and detected as previously described¹⁷. Probe and antibody details are given in the **Supplementary Methods**.

RT-PCR RNA was prepared from microdissected cortical and hippocampal tissue from E16.5 embryos or from P0 cortical tissue using Trizol reagent (Invitrogen), and cDNA was prepared from this RNA using the Superscript III first strand synthesis kit (Invitrogen). PCR primers for *Gap43*, *Robo1*, *Slit2*, *Fgfr2* and *Gapdh* were designed with the PRIMER 3 program and published database sequences (available upon request).

Slice culture, cortical explant culture. Telencephalic slice cultures were prepared as described in **Supplementary Methods**. PKH26 (Sigma) was applied over the ventricular zone in the coronal slice with a picoinjector fitted with a fine glass tip and, in some cases, FGF- or BSA-soaked beads were inserted into the dorsal side of the explant culture with a tungsten needle. Slice cultures were removed from the incubator and visualized by fluorescent and bright-field microscopy at 1-h, 24-h and 48-h time points.

Dorsal cortical explants were dissected from the E13.5 mouse telencephalon (FVB strain, **Supplementary Methods**). After 16 h in culture, heparin acrylic beads (Sigma) presoaked with either 20 μ M FGF2 (18 kDa, Invitrogen), 20 μ M FGF8b (R&D Systems) or 20 μ M BSA (Sigma) were embedded into these explants. BrdU labeling was performed by adding 0.1 mM BrdU (Sigma) to the culture media. Fixed explants were frozen, sectioned at 10 μ m and

analyzed by immunohistochemistry. For details regarding cell counting, see **Supplementary Methods**.

Morphometry and statistical analysis. Unbiased estimates for the density of GFAP⁺ or BrdU⁺ cells in tissue sections were obtained using a computer coupled to a Zeiss Axioskope 2 Mot Plus equipped with a motorized stage, running the StereoInvestigator software (Microbrightfield; **Supplementary Methods**). Data were analyzed by ANOVA or Student's *t*-test using the DataDesk statistical program. The number of samples is specified in each case in the figure legends. *Post-hoc* analyses were performed via the Scheffé *post-hoc* test.

Note: Supplementary information is available on the Nature Neuroscience website.

ACKNOWLEDGMENTS

We thank A. Uchida for explant preparation and valuable discussions; S.L. Ellis and J. Silbereis for technical assistance; R. Slack (University of Ottawa, Ottawa, Ontario) for the Nestin-Cre mice; J. Marth (University of California San Diego) for the Syn1-Cre mice; J. Partanen (Institute of Biotechnology, University of Helsinki, Helsinki, Finland) for the FGF1^{fl/fl} mice; D. Ornitz (Washington University Medical School, Saint Louis) for the FGF2^{fl/fl} mice; K. Kwan (Yale University, New Haven) for generating pCGLH; E. Anton (University of North Carolina, Chapel Hill, North Carolina) for providing pBLBP-EGFP; and J. Miyazaki (Osaka University, Osaka, Japan) for providing pCAGGS. We are grateful to M. Tessier-Lavigne (Genentech, South San Francisco) for probes and J. Rubenstein (University of California San Francisco) for sharing data. This work was supported by the US National Institutes of Health (grants MH067715, NS35476, 5T32-MH18268, NS054273 and HD045481) and the National Alliance for Research on Schizophrenia and Depression Foundation.

COMPETING INTERESTS STATEMENT

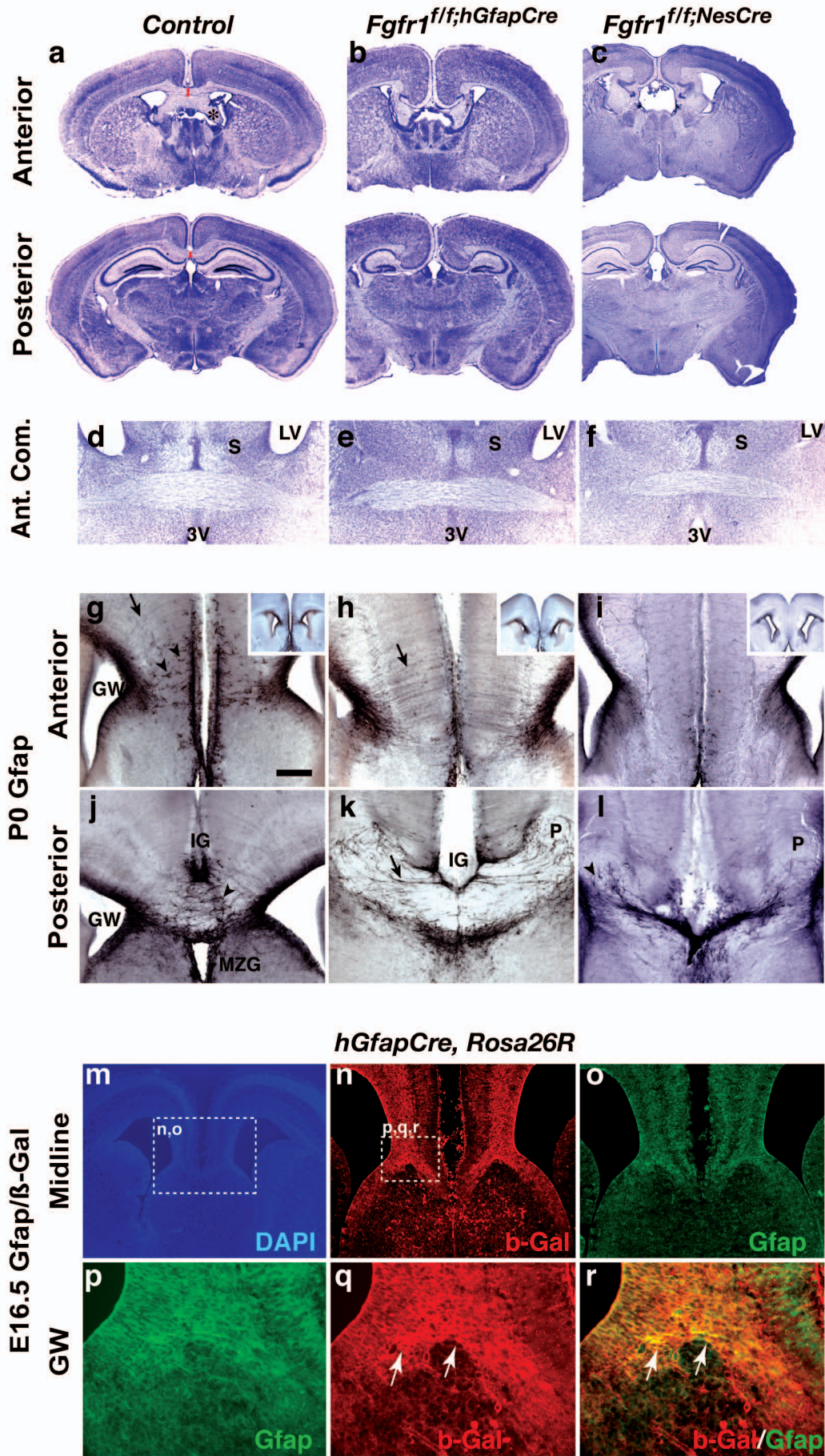
The authors declare that they have no competing financial interests.

Published online at <http://www.nature.com/natureneuroscience>

Reprints and permissions information is available online at <http://npg.nature.com/reprintsandpermissions/>

- Schmechel, D.E. & Rakic, P. A Golgi study of radial glial cells in developing monkey telencephalon: morphogenesis and transformation into astrocytes. *Anat. Embryol. (Berl.)* **156**, 115–152 (1979).
- Pixley, S.K.R. & de Vellis, J. Transition between immature glia and mature astrocytes studied with a monoclonal antibody to vimentin. *Dev. Brain Res.* **15**, 201–209 (1984).
- Mission, J.P., Takahashi, T. & Caviness, V.S., Jr. Ontogeny of radial and other astroglial cells in murine cerebral cortex. *Glia* **4**, 138–148 (1991).
- Shu, T., Puche, A.C. & Richards, L.J. Development of midline glial populations at the cortico-septal boundary. *J. Neurobiol.* **57**, 81–94 (2003).
- Silver, J., Edwards, M.A. & Levitt, P. Immunocytochemical demonstration of early appearing astroglial structures that form boundaries and pathways along axon tracts in the fetal brain. *J. Comp. Neurol.* **328**, 415–436 (1993).
- Shu, T. & Richards, L.J. Cortical axon guidance by the glial wedge during the development of the corpus callosum. *J. Neurosci.* **21**, 2749–2758 (2001).
- Silver, J. & Ogawa, M.Y. Postnatally induced formation of the corpus callosum in acallosal mice on glia-coated cellulose bridges. *Science* **220**, 1067–1069 (1983).
- Shu, T., Butz, K.G., Plachez, C., Gronostajski, R.M. & Richards, L.J. Abnormal development of forebrain midline glia and commissural projections in *Nfia* knock-out mice. *J. Neurosci.* **23**, 203–212 (2003).
- Kriegstein, A.R. & Gotz, M. Radial glia diversity: a matter of cell fate. *Glia* **43**, 37–43 (2003).
- Qian, X., Davis, A.A., Goderie, S.K. & Temple, S. FGF2 concentration regulates the generation of neurons and glia from multipotent cortical stem cells. *Neuron* **18**, 81–93 (1997).
- Song, M.R. & Ghosh, A. FGF2-induced chromatin remodeling regulates CNTF-mediated gene expression and astrocyte differentiation. *Nat. Neurosci.* **7**, 229–235 (2004).
- Morrow, T., Song, M.R. & Ghosh, A. Sequential specification of neurons and glia by developmentally regulated extracellular factors. *Development* **128**, 3585–3594 (2001).
- Ornitz, D. & Itoh, N. Fibroblast growth factors. *Genome Biol.* **2**, 3005–3012 (2001).
- Itoh, N. & Ornitz, D.M. Evolution of the *Fgf* and *Fgfr* gene families. *Trends Genet.* **20**, 563–569 (2004).
- Storm, E.E., Rubenstein, J.L. & Martin, G.R. Dosage of FGF8 determines whether cell survival is positively or negatively regulated in the developing forebrain. *Proc. Natl. Acad. Sci. USA* **100**, 1757–1762 (2003).
- Vaccarino, F.M. *et al.* Changes in cerebral cortex size are governed by fibroblast growth factor during embryogenesis. *Nat. Neurosci.* **2**, 246–253 (1999).
- Raballo, R. *et al.* Basic fibroblast growth factor (Fgf2) is necessary for cell proliferation and neurogenesis in the developing cerebral cortex. *J. Neurosci.* **20**, 5012–5023 (2000).
- Garel, S., Huffman, K.J. & Rubenstein, J.L.R. Molecular regionalization of the neocortex is disrupted in *Fgf8* hypomorphic mutants. *Development* **130**, 1903–1914 (2003).
- Fukuchi-Shimogori, T. & Grove, E.A. Neocortex patterning by the secreted signaling molecule FGF8. *Science* **294**, 1071–1074 (2001).
- Ohkubo, Y., Chiang, C. & Rubenstein, J.L. Coordinate regulation and synergistic actions of BMP4, SHH and FGF8 in the rostral prosencephalon regulate morphogenesis of the telencephalic and optic vesicles. *Neuroscience* **111**, 1–17 (2002).
- Gregg, C. & Weiss, S. Generation of functional radial glial cells by embryonic and adult forebrain neural stem cells. *J. Neurosci.* **23**, 11587–11601 (2003).
- Yoon, K. *et al.* Fibroblast growth factor receptor signaling promotes radial glial identity and interacts with Notch1 signaling in telencephalic progenitors. *J. Neurosci.* **24**, 9497–9506 (2004).
- Ohkubo, Y., Uchida, A.O., Shin, D., Partanen, J. & Vaccarino, F.M. Fibroblast growth factor receptor 1 is required for the proliferation of hippocampal progenitor cells and for hippocampal growth in mouse. *J. Neurosci.* **24**, 6057–6069 (2004).
- Dode, C. *et al.* Loss-of-function mutations in *FGFR1* cause autosomal dominant Kallmann syndrome. *Nat. Genet.* **33**, 463–465 (2003).
- Pirvola, U. *et al.* FGFR1 is required for the development of the auditory sensory epithelium. *Neuron* **35**, 671–680 (2002).
- Malatesta, P. *et al.* Neuronal or glial progeny: regional differences in radial glia fate. *Neuron* **37**, 751–764 (2003).
- Graus-Porta, D. *et al.* Beta1-class integrins regulate the development of laminae and folia in the cerebral and cerebellar cortex. *Neuron* **31**, 367–379 (2001).
- Ozaki, H.S. & Wahlsen, D. Prenatal formation of the normal mouse corpus callosum: a quantitative study with carbocyanine dyes. *J. Comp. Neurol.* **323**, 81–90 (1992).
- Minowada, G. *et al.* Vertebrate Sprouty genes are induced by FGF signaling and can cause chondrodysplasia when overexpressed. *Development* **126**, 4465–4475 (1999).
- Maruoka, Y. *et al.* Comparison of the expression of three highly related genes, *Fgf8*, *Fgf17* and *Fgf18*, in the mouse embryo. *Mech. Dev.* **74**, 175–177 (1998).
- Crossley, P.H. & Martin, G.R. The mouse *FGF8* gene encodes a family of polypeptides and is expressed in regions that direct outgrowth and patterning in the developing embryo. *Development* **121**, 439–451 (1995).
- Shu, T., Sundaresan, V., McCarthy, M.M. & Richards, L.J. *Slit2* guides both precrossing and postcrossing callosal axons at the midline *in vivo*. *J. Neurosci.* **23**, 8176–8184 (2003).
- Zhu, Y. *et al.* Ablation of NF1 function in neurons induces abnormal development of cerebral cortex and reactive gliosis in the brain. *Genes Dev.* **15**, 859–876 (2001).
- Soriano, P. Generalized *lacZ* expression with the ROSA26 Cre reporter strain. *Nat. Genet.* **21**, 70–71 (1999).
- Hasegawa, H. *et al.* Laminar patterning in the developing neocortex by temporally coordinated fibroblast growth factor signaling. *J. Neurosci.* **24**, 8711–8719 (2004).
- Yu, K., Herr, A.B., Waksman, G. & Ornitz, D.M. Loss of fibroblast growth factor receptor 2 ligand-binding specificity in Apert syndrome. *Proc. Natl. Acad. Sci. USA* **97**, 14536–14541 (2000).
- Meyers, E.N., Lewandoski, M. & Martin, G.R. An FGF8 mutant allelic series generated by Cre- and FLP-mediated recombination. *Nat. Genet.* **18**, 136–141 (1998).
- Huffman, K.J., Garel, S. & Rubenstein, J.L. FGF8 regulates the development of intra-neocortical projections. *J. Neurosci.* **24**, 8917–8923 (2004).
- Shanmugalingam, S. *et al.* *Ace*/FGF8 is required for forebrain commissure formation and patterning of the telencephalon. *Development* **127**, 2549–2561 (2000).
- Klambt, C., Glazer, L. & Shilo, B.Z. *breathless*, a *Drosophila* FGF receptor homolog, is essential for migration of tracheal and specific midline glial cells. *Genes Dev.* **6**, 1668–1678 (1992).
- Williams, E.J., Furness, J., Walsh, F.S. & Doherty, P. Activation of the FGF receptor underlies neurite outgrowth stimulated by L1, N-CAM, and N-Cadherin. *Neuron* **13**, 583–594 (1994).
- Webber, C.A., Hyakutake, M.T. & McFarlane, S. Fibroblast growth factors redirect retinal axons *in vitro* and *in vivo*. *Dev. Biol.* **263**, 24–34 (2003).
- Rash, B.G. & Richards, L.J. A role for cingulate pioneering axons in the development of the corpus callosum. *J. Comp. Neurol.* **434**, 147–157 (2001).
- Shin, D.M. *et al.* Loss of glutamatergic pyramidal neurons in frontal and temporal cortex resulting from attenuation of FGFR1 signaling is associated with spontaneous hyperactivity in mice. *J. Neurosci.* **24**, 2247–2258 (2004).
- Cheng, Y., Black, I.B. & DiCicco-Bloom, E. Hippocampal granule neuron production and population size are regulated by levels of bFGF. *Eur. J. Neurosci.* **15**, 3–12 (2002).
- Faux, C.H., Turnley, A.M., Epa, R., Cappai, R. & Bartlett, P.F. Interactions between fibroblast growth factors and Notch regulate neuronal differentiation. *J. Neurosci.* **21**, 5587–5596 (2001).
- Hebert, J.M., Lin, M., Partanen, J., Rossant, J. & McConnell, S.K. FGF signaling through FGFR1 is required for olfactory bulb morphogenesis. *Development* **15**, 1101–1111 (2003).
- Zhuo, L. *et al.* hGFAP-cre transgenic mice for manipulation of glial and neuronal function *in vivo*. *Genesis* **31**, 85–94 (2001).
- Chen, J.G., Rasin, M.R., Kwan, K.Y. & Sestan, N. Zfp312 is required for subcortical axonal projections and dendritic morphology of deep-layer pyramidal neurons of the cerebral cortex. *Proc. Natl. Acad. Sci. USA* **102**, 17792–17797 (2005).
- Schmid, R.S., Yokota, Y. & Anton, E.S. Generation and characterization of brain lipid-binding protein promoter-based transgenic mouse models for the study of radial glia. *Glia* **53**, 345–351 (2006).

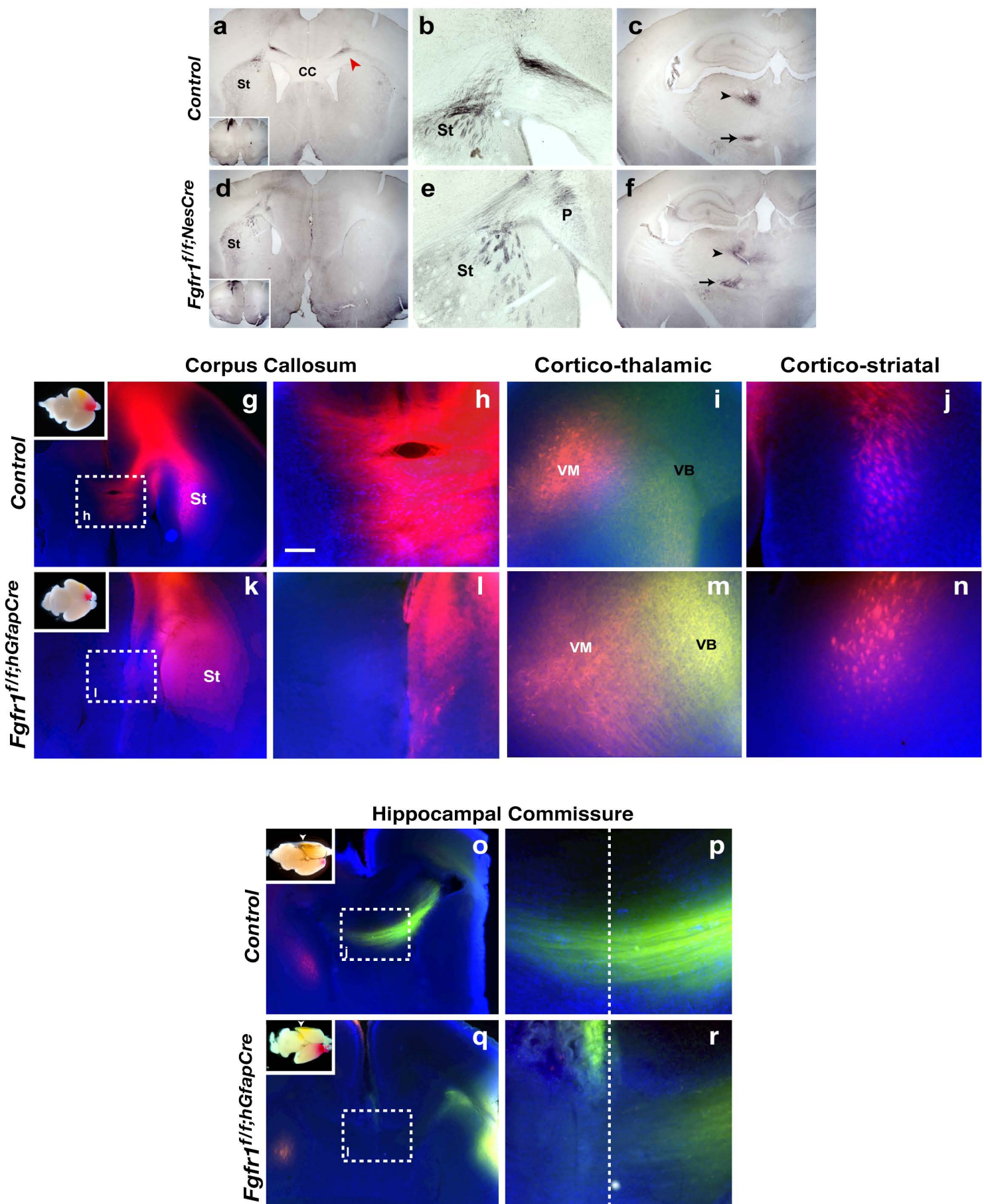
Smith et al., Supplemental Figure 1



Supplemental Figure 1. Lack of dorsal telencephalic commissures in *Fgfr1* mutants correlates with absence of the IG. (a–f) Cresyl violet staining in adult control (a,d), *Fgfr1^{fl/f};hGfapCre* (b,e) and *Fgfr1^{fl/f};NesCre* mice (c,f) at levels used for commissure measurements, showing the absence of corpus callosum (a–c, red arrows) with preservation of anterior commissure (d–f) in mutant mice as compared to controls. (g–l) Gfap staining at P0 just anterior (g–i) and 200 μ m posterior (j–l) to the beginning of the corpus callosum in control (g,j), *Fgfr1^{fl/f};hGfapCre* (h,k) and *Fgfr1^{fl/f};NesCre* mice (i,l). (m–r) Cre recombination occurs within Gfap+ cells of the GW in *hGfapCre;Rosa 26R* (+/-) mouse telencephalon at E16.5. DAPI staining (m) shows the location of the higher magnification images in (n–o). Immunohistochemistry for β -Gal (n,q) and Gfap (o,p) in the dorsomedial cortical wall and septum, merged images in (r). Scale bar is 200 μ m in g–l, 380 μ m in m, 190 μ m in n,o, 47 μ m in p–q.

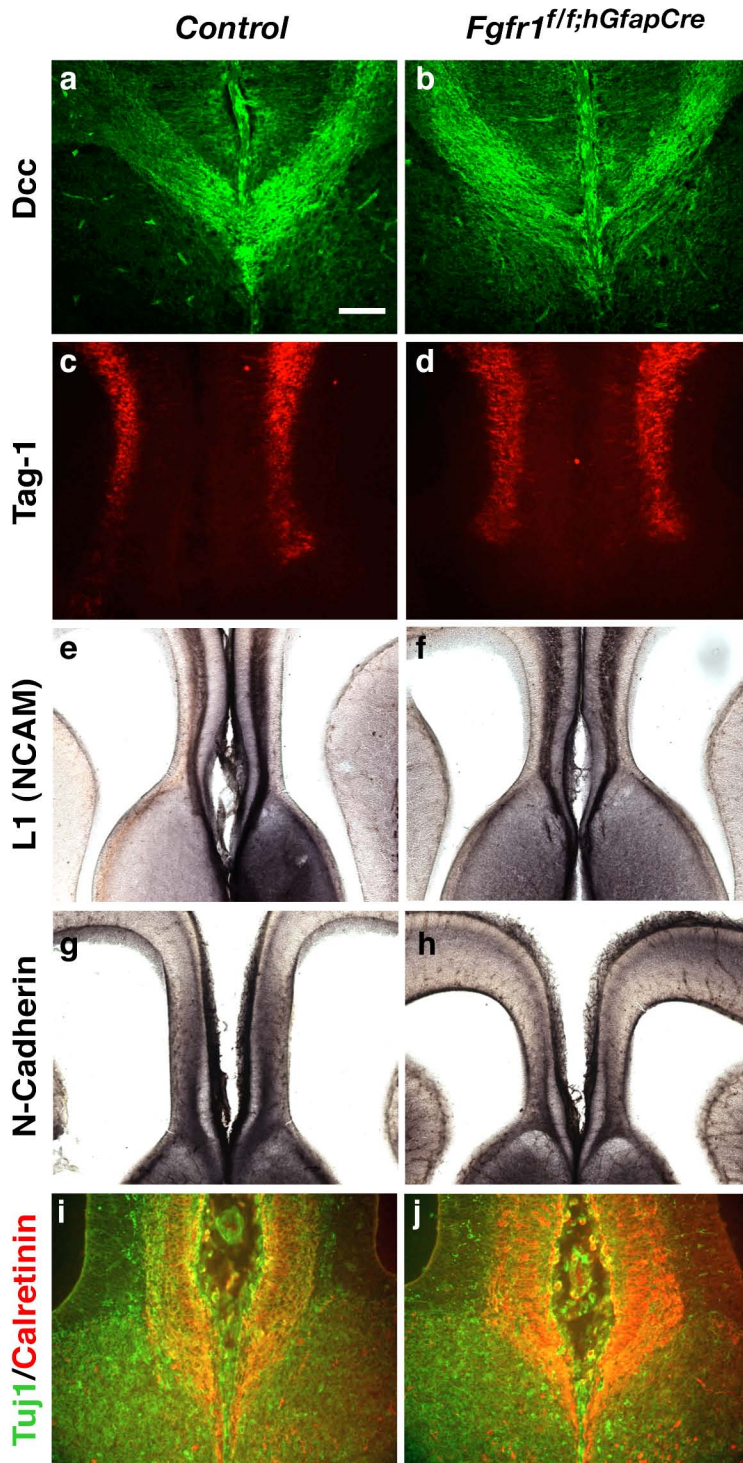
GW, glial wedge; S, septum; LV, lateral ventricle; MZ, midline zipper glia; 3V, 3rd ventricle.

Smith et al., Supplemental Figure 2



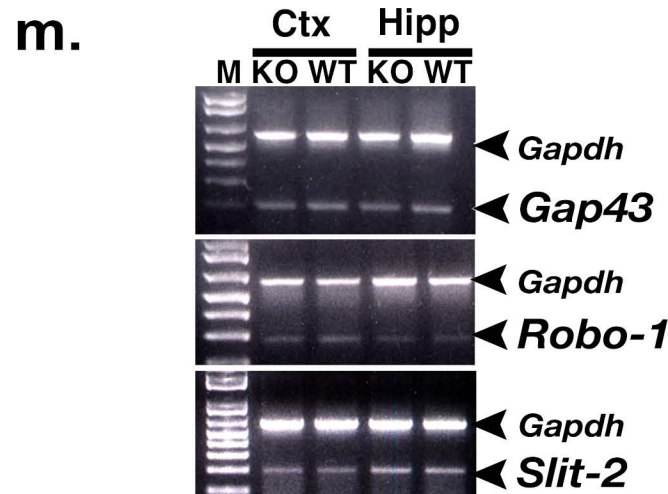
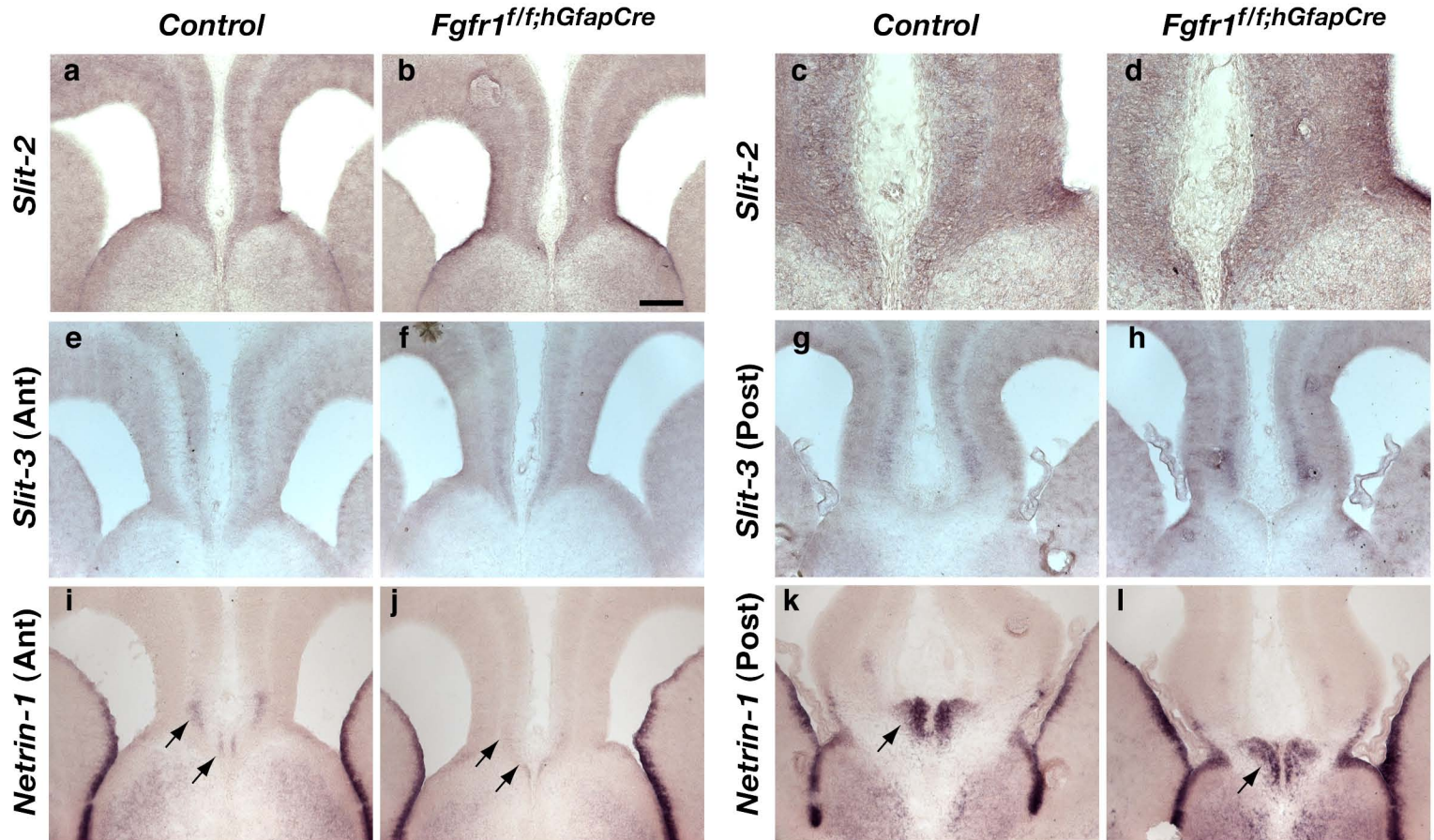
Supplemental Figure 2. *Fgfr1* mutants have specific deficits in the formation of dorsal telencephalic commissures. (a–f) Representative BDA tracing in control and *Fgfr1^{f/f};NesCre* adults. (b) and (e) are 4x magnifications of (a) and (d), respectively. BDA injections into the frontal cortex (insets) label fibers of the corpus callosum and contralateral white matter in control (a,b) but not in *Fgfr1* mutant mice (d,e). However, the ipsilateral white matter and striatum (St) (b,e) and cortical projections to the thalamic medial dorsal (arrowhead) and ventromedial nuclei (small arrow) (c,f) are labeled in both control and mutant mice. P, Probst bundles; red arrowhead, labeled fibers in contralateral white matter. (g–n) Axonal tracing from motor (Dil, red) or somatosensory (DiA, yellow-green) cortex in control (g–j) and *Fgfr1^{f/f};hGfapCre* (k–n) neonatal mice. Implant sites shown in inside panel in (g,k). (h,i) High magnification of the midline showing absence of callosal axons in *Fgfr1^{f/f};hGfapCre* mice. Axons from motor cortex innervate the ventral-medial (VM) thalamic nuclei, and axons from somatosensory cortex innervate ventro-basal (VB) nuclear complex in both controls (i) and *Fgfr1^{f/f};hGfapCre* (m) mice. Projections from motor cortex innervate the dorsolateral striatum in both control (j) and *Fgfr1^{f/f};hGfapCre* (n) mice. (o–r) DiA (yellow-green signal) was implanted into the hippocampus of control (o,p) and *Fgfr1^{f/f};hGfapCre* (q,r) brains. Inserts in (o,p) show implantation sites. (p,r) High magnification of the midline showing absence of hippocampal commissural axons in *Fgfr1^{f/f};hGfapCre* mice. Scale bar is 400 μm in g,k,o,q and 100 μm in the other panels.

Smith et al., Supplemental Figure 3



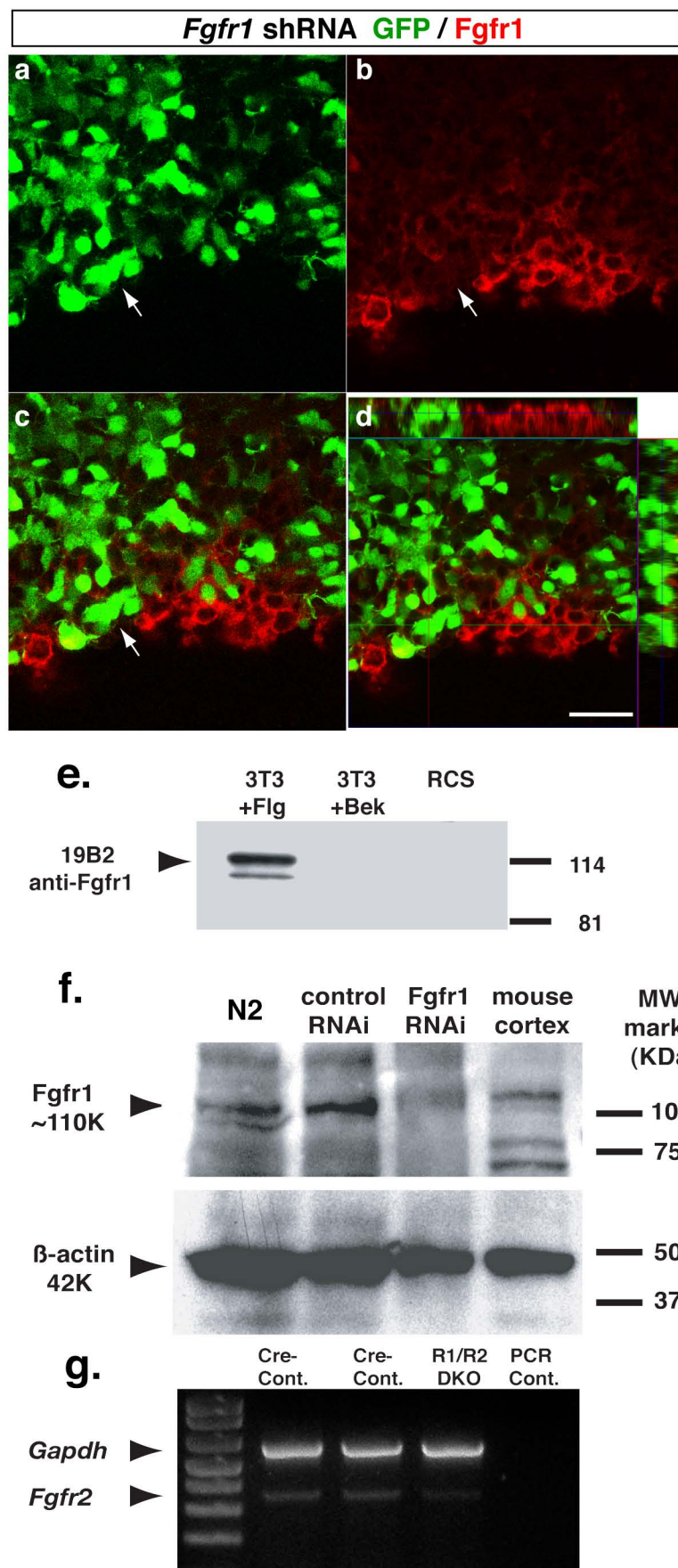
Supplemental Figure 3. *Fgfr1* mutation does not alter the expression of neuronal factors implicated in midline axon guidance. (a,b) Immunohistochemistry for Dcc (a–b), Tag-1 (c–d), L1 (NCAM) (e–f), N-Cadherin (g–h) in *Fgfr1*^{f/f};hGfpCre embryos (b,d,f,h) is comparable to that of control embryos (a,c,e,g) at E16.5. The Dcc-labeled commissural axons in *Fgfr1*^{f/f};hGfpCre mice (b) are less fasciculated as compared to those in controls (a) and do not appear to cross the midline. (i,j) Tuj-1 (Green) and Calretinin (Red) double immunohistochemistry at E16.5 in control (i) and *Fgfr1*^{f/f};hGfpCre (j) embryos. As previously reported, a large number of calretinin⁺ interneurons are present near the IG and in the glial sling. Scale bar is 100 μ m in a–d and i,j, 200 μ m e,h.

Smith et al., Supplemental Figure 4



Supplemental Figure 4. In situ hybridization and RT-PCR of axon guidance molecules in control and hGfap/Cre *Fgfr1* mutant embryos. (a–l) Slit-2 (a–d), Slit-3 (e–h), and Netrin-1 (i–l) in situ hybridization in control (a,c,e,g,i,k) and *Fgfr1^{f/f};hGfapCre* (b,d,f,h,j,l) embryos at E16.5. Arrows, prospective IG. Scale bar is 200 μ m a,b and e–l, 70 μ m in c,d. (m) *Gap43*, *Robo-1*, and *Slit-2* expression levels are similar in control (WT) and *Fgfr1^{f/f};hGfapCre* (KO) embryos in microdissected CP (Ctx) and hippocampal ridge (Hipp) from E16.5 embryos, as detected by RT-PCR. The *Gapdh* gene was used as an internal control.

Smith et al., Supplemental Figure 5



Supplemental Figure 5. Decreased expression of Fgfr1 protein after shRNA knockdown and Fgfr2 mRNA in Fgfr2f/f;hGfapCre mice. (a-d) Double immunostaining for GFP (green) and Fgfr1 (19B2 antibody, red) in sections of E17.5 brains electroporated in utero at E14.5 with pCGLH vectors expressing or Fgfr1 shRNAs. Arrows, cells expressing the Fgfr1 shRNAs as revealed by GFP express little Fgfr1 immunoreactivity. (e) Western blot of lysates prepared from cell lines constitutively expressing Fgfr1 (3T3+Flg), Fgfr2 (3T3+ Bek) or Fgfr3 (RCS) probed with the Fgfr1 19B2 antibody. (f) Western blot of lysates prepared from native N2A cells (lane 1) or N2A cells electroporated with a mixture of 3 control shRNAs vectors (each harboring 4 mutations in the Fgfr1 targeting sequences) (lane 2) or a mixture of 3 shRNA vectors targeting Fgfr1 (lane 3). The last lane is an extract of mouse cortex. (g) Semiquantitative RT-PCR for Fgfr2 and Gapdh in cortical tissue extracts of Fgfr1;Fgfr2f/f;hGfapCre (R1/R2 DKO) mice and control littermates (Cre-cont.). Primers for the Fgfr2 gene were designed to amplify the region encompassed within the loxP sites. Scale bar is 12.5 μ m.

Supplemental Methods

Axonal Tracing

Two hundred nanoliters of a 10% Biotinylated Dextran Amine (10,000 MW, Molecular Probes) solution in PB buffer was injected into the brains of adult animals, deeply anesthetized with ketamine and xylazine (100 mg/kg and 10 mg/kg). Injections were performed in a stereotaxic surgery restraint system equipped with a nanoinjector (Stoelting) using the following coordinates: Anterior-Posterior +1.94 mm, Medial-Lateral +.5 mm, Dorsal-Ventral –1.40 mm (all coordinates taken from bregma). Seven days after injection, animals were sacrificed by intracardial perfusion with 4% paraformaldehyde (PFA) in PBS. Brains were cryoprotected and sectioned at 50 μ M on a cryostat. BDA was detected with avidin-HRP and DAB (Vector) or FITC-avidin DCS (Vector) and analyzed by microscopy.

For tracing with Dil and DiA (Molecular Probes), neonatal mice (P0-P1) were sacrificed by intracardial perfusion, and brains were postfixed in 4%PFA at 4°C for three days. Pulled glass pipette tips previously coated with Dil or DiA were implanted into anterior cingulate, somatosensory cortex, or the hippocampus. Brains were embedded in agar and incubated at 37°C for 6-10 weeks, after which implants were removed, and pictures were taken to document implant site. Brains were sectioned in agar at 100 μ M on a VT1000 Vibratome (Leica), mounted on slides and counter stained with DAPI.

In Utero Electroporation and RNAi. For *in utero* gene transfer by electroporation, 1-2 µl of DNA solution (4 mg/ml) was injected into the lateral ventricle and electroporated (five 50 ms square pulses of 40 V with 950 ms intervals). For RNA interference experiment, a template for short hairpin RNA (shRNA) synthesis was made by annealing a pair of oligonucleotides representing the sense and antisense strands of the target sequence. The oligonucleotides sequences chosen for *Fgfr1* targeting were: 5'-AGGTTTCTGTTTAGGCCT-3'; 5'-GGCCAGACAACCTTGCCGTA-3'; 5'-CCAGTACTCACCCAGCTT-3'. These oligos target, respectively, the 3'-UTR (bp 2624 to 2641), the second the extracellular IG-like region (bp 657 to 675) and the third the intracellular tyrosine kinase domain (bp 2077 to 2093) (all bases are given with reference to Genbank accession no. BCO3347). BLAST searches indicated that none of the oligonucleotides sequences chosen had any significant matches to any other known mammalian genes. The annealed template was cloned into pCGLH shRNA vector coexpressing GFP. pCGLH was created by replacing RFP from pCRLH with GFP (Chen et al. 2005. PNAS 102:17792-17797). Mutated (4 mutations per sequence) *Fgfr1* targeting sequences were used as a control. The sequences of point-mutated control oligos were: 5'-AGATTACTCTTTACGCCT-3'; 5'-GGCATACCACTCGCCATA-3'; 5'-CCATTAATCACTCCGCTT-3'. Equal amounts of the three shRNA vectors targeting the *Fgfr1* gene or of the three control vectors with mutated shRNA sequences were injected. Empty pCGLH shRNA vector coexpressing GFP was also injected as additional controls in separate experiments. Cells expressing

shRNA were reliably identified by the co-expression of GFP. To assess the degree of *Fgfr1* knockdown, FACS sorted transfected Neuro2a cells or untransfected Neuro2a cells were homogenized in 6x SDS sample buffer (12% SDS, 600mM DTT, 300mM Tris-HCl, pH 6.8), and used for Western blotting with anti-FGFR1 antibodies (Yu302, gift of J. Schlessinger or 19B2, UBI) or an anti- β -actin antibody as previously described (Ohkubo et al. 2005. J Neurosci 24:6057-6059) (**Supplementary Fig. 5f**). To assess *Fgfr1* knockdown *in vivo*, sections obtained from shRNA electroporated brains were reacted with the 19B2 monoclonal antibody (**Supplementary Fig. 5a-e**). Robust inhibition of *Fgfr1* protein expression was obtained with either method by transfecting shRNA targeted to *Fgfr1*, while control shRNA vectors produced no change in *Fgfr1* expression as compared to untransfected cells (**Supplementary Fig. 5**). Fluorescent images were obtained using a Zeiss LSM500 confocal microscope. In selected cases, GFP was visualized using diaminobenzidine immunohistochemistry with anti-GFP antibody (1:3,000; A11122, Molecular Probes).

***In situ* Hybridization and Immunohistochemistry**

The following cDNA were used as probes: *Fgfr1* (exon 9-15; comprising the intracellular portion of *Fgfr1*, which is deleted in hGfap/Cre KO animals); *mSprouty1* (complete protein coding region and 3'UTR; Minowada et al., 1999. Development 126:4465-4475); *FGF-8* (3'UTR and C-terminal coding sequences; Crossley and Martin. 1995. Development 121:439-451); *Slit-2* and *Slit-3* (Brose

et al. 1999. Cell 96:796-806), and *Netrin-1* (Serafini et al. 1996. Cell:86:1001-1014) .

The following primary antibodies were used for immunohistochemistry:

β galactosidase (Cappel or Promega), Blbp (gift from Dr. Nathaniel Heintz or Chemicon), BrdU (Accurate Chemical), Calretinin (Swant), Dcc (BD Pharmingen), Fgfr1 (19B2, Upstate), Gfap (DAKO), Glast (gift from Dr. M. Watanabe), Nestin (Chemicon), PCNA (Upstate), L1 (Chemicon), MNCD2 (N-cadherin, gift from Dr. M. Takeichi), Tuj1 (Promega), RC2 and Tag1 (Developmental Studies Hybridoma Bank).

Slice Culture, Cortical Explant Culture

Telencephalic slices culture was performed as previously described (Anderson et al. 1997. Science 278:474-476). Embryonic explants from the dorsal telencephalon were prepared as described (Furuta et al. 1997. Development 124: 2203-2212). Dorsal cortical explants were dissected from the E13.5 mouse telencephalon (FVB strain). Cortical tissue was carefully trimmed to remove the ganglionic eminences and developing hippocampi. After 16 hours in culture, heparin acrylic beads (Sigma) presoaked for 30 minutes with either 20 μ M FGF2 (18 kDa, Invitrogen), 20 μ M Fgf8b (R&D Systems, MN) or 20 μ M BSA (Sigma) were embedded into these explants. BrdU labeling was performed by adding 0.1mM BrdU (Sigma) to the culture media prior to returning explants to the incubator. Fixed explant tissue was sectioned at 10 μ m and analyzed by immunohistochemistry. PCNA and BrdU positive cells were counted in 2 bins of

tissue per experiment encompassing the VZ and the IZ/CP. In the VZ, an average of 97 DAPI-stained cells per experiment over a total area of $125 \mu\text{m}^2$ were evaluated, among which (depending upon the treatment) an average of 54 to 73 were stained for PcnA, and 35 to 40 were stained for BrdU. In the IZ/CP an average of 260 DAPI-stained cells per experiment over a total area of $375 \mu\text{m}^2$ were evaluated, among which (depending upon the treatment) an average of 28 to 165 were stained for PcnA, and 5 to 78 were stained for BrdU. Counts were normalized by the area to obtain cell density. Number of independent experiments: $n = 4$ control, $n = 5$ FGF2, $n = 4$ FGF8.

Cell counting

Unbiased estimates for density of Gfap or BrdU-positive cells were obtained using a computer coupled to a Zeiss Axioskope 2 Mot Plus equipped with a motorized stage, running the StereoInvestigator software (Microbrightfield, Colchester, VT). Nuclear profiles were counted in 3-dimensional counting boxes, using a randomly placed sampling grid of $500 \times 350 \mu\text{m}$ on the cerebral cortex and $100 \times 100 \mu\text{m}$ on the SVZ. Counting boxes ($100 \times 100 \times 8 \mu\text{m}$) were placed in $1 \mu\text{m}$ below the surface at each of the grid intersection points. Cells immunoreactive for Gfap were only counted if they overlapped a DAPI-stained cell nucleus.